# Chapter 2

# Solar and Stellar Structure

## 2.1 The Sun as a star

All stars in our galaxy have been formed from clouds of gas and dust. Eventually, gravity causes the clouds to collapse, and since the clouds are spinning, centrifugal forces result in accretion disks. The material that concentrates into the disk centers forms new stars. While the stars continue to grow, lumps form in the disks which will ultimately become planets. The disks become thinner as more material falls onto the stars and the protoplanets.

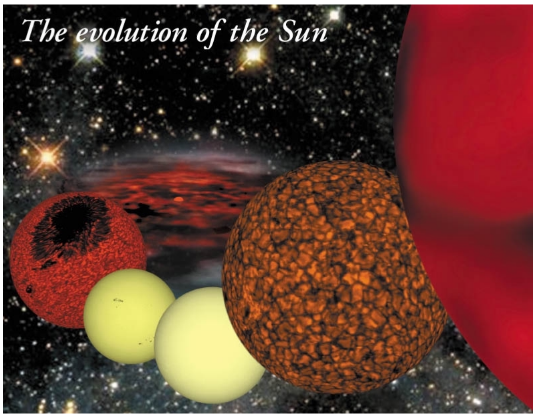


Our sun was formed some 4.5 billion (american) / 4.5 milliard (british) years ago. The first tens of millions of years, the sun was extremely magnetically active. Gigantic starspots covered its surface, at times even in its polar regions. Then, the sun settled into a long stable life as a common, yellow star (spectral class G2V; G2 means that it has a surface temperature of approximately 5780 K). In the next 6.5 billion/milliard years, the activity continues to subside, and the sun will slightly increase in size and brightness. Then it will run out of the hydrogen that fuels the fusion reactor in its core. For a while it will find new ways of nuclear fusion, as it swells up to an orange giant. Because surface gravity weakens as the star grows, the convective bubbles (that span only approximately 1000 km on the present sun) will become much larger. Within the following few million years, the sun will grow into a huge red giant, one hundred times its present size. In that phase, only a handful of huge convection cells will cover its surface, that will be undulating by millions of miles as the convective flows evolve; the Sun will generally look oddly distorted from the average spherical state shown on the front. This brief phase heralds the end of the earth, which will be cooked in the intense radiation, and most likely be engulfed by our star. After that, the sun will shrink to a size only somewhat larger than the earth, and eventually slowly fade out. (The evolution of the Sun, image and slightly edited text are from Karel Schrijver's Cool Star Homepage at `http://www.lmsal.com/ schryver/Public/homepage/coolstarimages.html`).

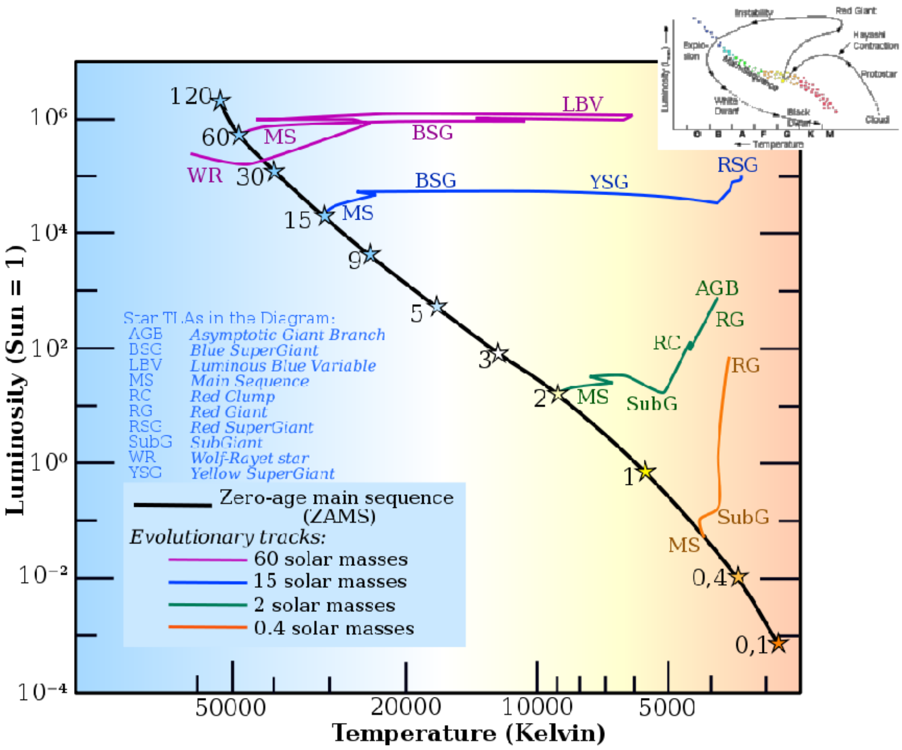


Figure 2.1: Stellar evolution (H-R diagram by Rursus, Wikimedia Commons; insert solar track image from Gene Smith's Astronomy Tutorial)

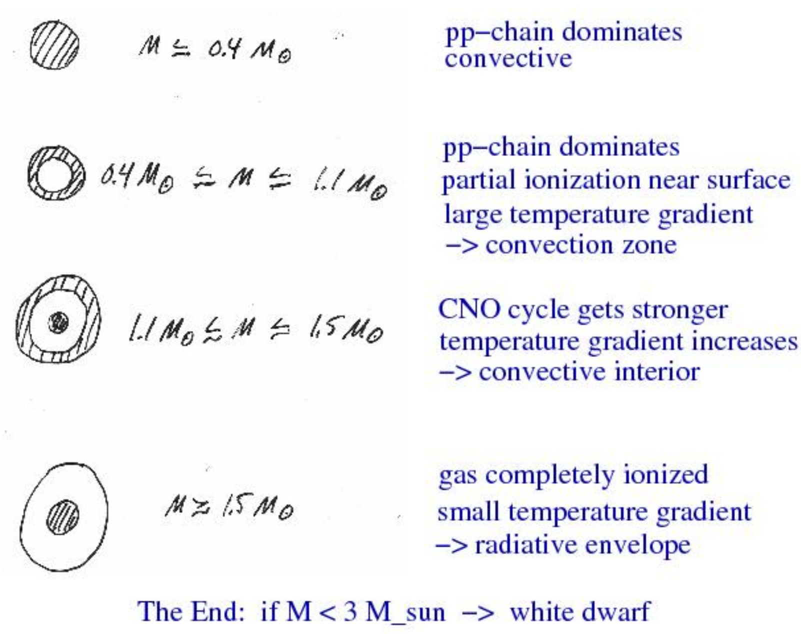


Figure 2.2: Stellar structure during the main sequence, for stars with different masses.

## 2.2 Energy production

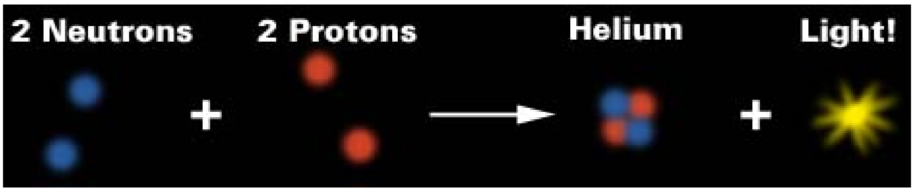


The proton-proton chain reaction (pp-chain) goes as follows:

$^1H + {}^1H \longrightarrow {}^2H + e^+ + \nu_e$

$(e^+ + e^- \longrightarrow 2\gamma)$

$^2H + {}^1H \longrightarrow {}^3He + \gamma$

$^3He + {}^3He \longrightarrow {}^4He + 2\ {}^1H$ **ppI**

The pp-chain is one of several fusion reactions by which stars convert hydrogen to helium. The first step involves the fusion of two hydrogen nuclei into deuterium, releasing a positron and a neutrino. The positron immediately annihilates with an electron, and their mass energy is carried off by two gamma ray photons. The deuterium produced in the first stage can then fuse with another hydrogen nuclei, to produce an isotope of helium, $^3$He. From here there are three possible ways to generate $^4$He, but the ppI chain is the most probable process in the Sun: the $^4$He is created from fusing two of the $^3$He that were produced in earlier processes. The ppI branch is dominant at temperatures of 10 – 14 MK. The temperature at the center of the sun is approximately 15 MK, and about 90% of the sun's energy production is from the ppI branch.

Comparing the mass of the final helium-4 atom with the masses of the four protons reveals that 0.7% of the mass of the original protons has been lost. This mass is converted into energy, in the form of gamma rays and neutrinos released during each of the individual reactions. The total energy we get in one whole pp-chain is 26.7 MeV.

We can write the difference in atomic mass units (AMU) as

$4 \times \mathrm{M}_H \approx 4 \times 1.0075$ AMU = 4.0300 AMU,
$\mathrm{M}_{He} \approx 4.0013$ AMU $\Longrightarrow \Delta\mathrm{M} = 0.0287$ AMU

$\Delta\mathrm{E} = \Delta\mathrm{M}c^2 = 0.0287\times1.6604\times10^{-27}\ \mathrm{kg} \times (2.99\times10^8\ \mathrm{m/s})^2 \approx 4.283\times10^{-12}\ \mathrm{J}$

To keep the sun's present luminosity $L_\odot$ we need

$$\frac{L_\odot}{\Delta E} \approx \frac{3.8 \times 10^{26}\ \mathrm{W}}{4.283 \times 10^{-12}\ \mathrm{J}} \approx 0.89 \times 10^{38}\ \mathrm{reactions/s} \tag{2.1}$$

One reaction uses four hydrogen nuclei: $4 \times 0.89 \times 10^{38} \approx 3.6 \times 10^{38}$ atoms/s

$$N_H \approx \frac{M_\odot}{m_H} \approx \frac{1.989 \times 10^{30}\ \mathrm{kg}}{1.6734 \times 10^{-27}\ \mathrm{kg/atom}} \approx 1.2 \times 10^{57}\ \mathrm{atoms} \tag{2.2}$$

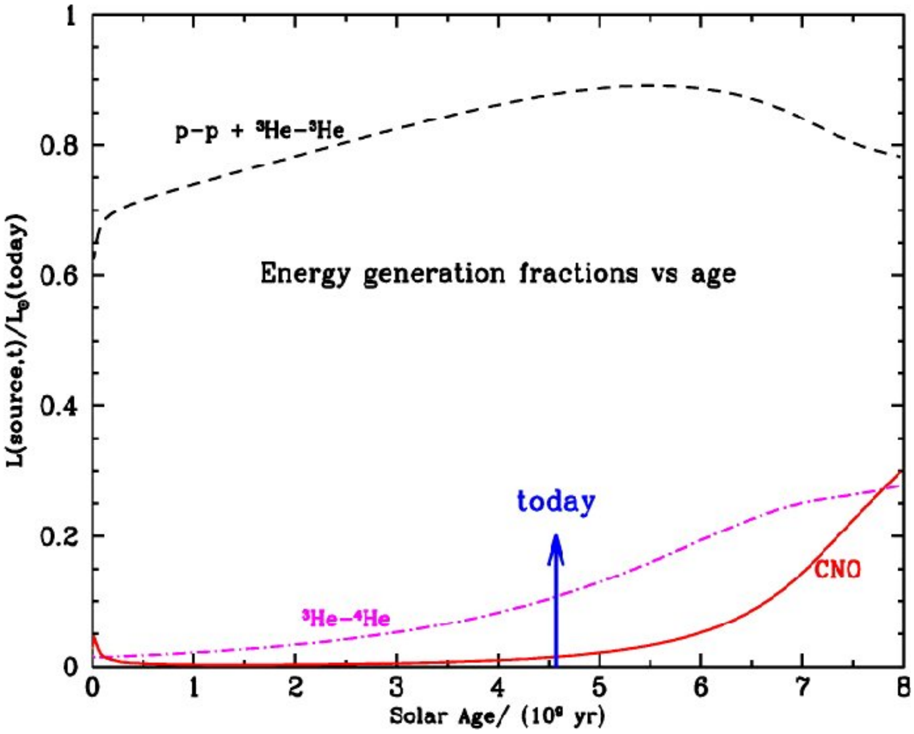


Figure 2.3: Fraction in the standard model of the solar luminosity produced by different nuclear fusion reactions vs. solar age. The luminosity generated by the p-p nuclear fusion branch that is terminated by the $^3$He-$^3$He reaction is marked by a dashed curve in the figure, and the luminosity produced by the p-p branches that proceed through the $^3$He-$^4$He reaction is denoted by a dot-dashed curve. The luminosity generation by the CNO cycle is indicated by a solid line. The unit of luminosity is the present-day total solar luminosity. At the present epoch, the p-p + 3He-3He reactions produce 87.8% of the solar luminosity and the branches terminating through the 3He-4He reaction generate 10.7% of the solar luminosity. The CNO cycle produces 1.5% of the present-epoch luminosity. (From Bahcall et al. ApJ 555, 990, 2001).

The sun could then be using its hydrogen supplies for

$$t_{max} \approx \frac{1.2 \times 10^{57}}{3.6 \times 10^{38}} \text{ s} \approx 10^{11} \text{ years.} \tag{2.3}$$

But, we believe that only 70% of the original solar mass was hydrogen, and only 10% of that hydrogen is usable in nuclear reactions. Hence, only about 0.7% of the total mass is converted into energy. For a main sequence star, we can use the timescale for nuclear reactions,

$$\tau_n = \frac{0.007 \times 0.1 M c^2}{L}. \tag{2.4}$$

For the sun, the timescale $\tau_n \approx 10^{10}$ years. The sun is estimated to be now about $4.5 - 4.6 \times 10^9$ years old. For more massive stars, that also have much higher luminosity, the timescale is much shorter.

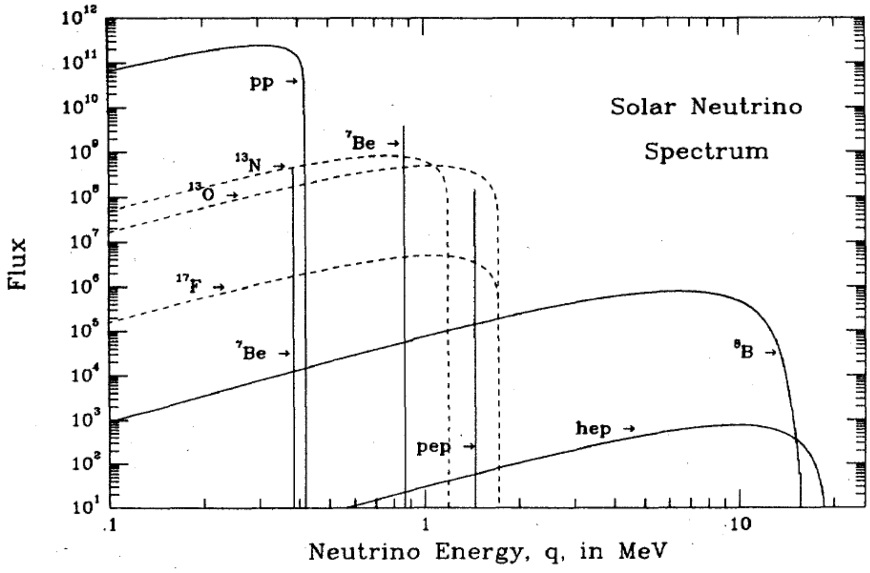


Figure 2.4: The energy spectrum and flux of solar neutrinos which should be received at earth according to the standard solar model of Bahcall and Ulrich. It can be seen that the neutrinos from $^{7}$B and $p\,e^{-}\,p$ have discrete energies and the others have continuous distribution. The majority of high-energy neutrinos are released by decay of $^{8}$B (From Bahcall and Ulrich, Rev. Modern Phys. 60, 297, 1988).

## 2.3 Neutrino problem

The neutrinos emitted in the first reaction of the pp-chain can have energy values between zero and 0.42 MeV. The decay of $^{8}$B can produce neutrinos with a maximum energy of about 15 MeV. All neutrinos interact weakly with matter, but the probability of absorption increases with energy. Despite the large value of mean free path, we should observe neutrinos (when they interact with matter at earth) because there are so many of them. There should be something like $10^{15}$ $m^{-2}$ $s^{-1}$ reaching the earth. A neutrino detector should then observe about one per month per cubic meter of the detector.

Neutrino detections are measured in solar neutrino unit, SNU, which is equal to $10^{-36}$ captures per target atom per second. The original theoretical detection rate was estimated to be about 30 SNU (Bahcall, 1966), but in the 1990s this value was lowered to 8 – 6 SNU. The experimental result is about 2 SNU. So, is the standard solar model wrong, or are neutrinos behaving oddly?

The news in June 2001 stated: the neutrino problem has been solved!

According to the standard model of particle physics, there are three different kinds of neutrinos: electron neutrinos, muon neutrinos, and tau neutrinos. Already in late 1960s it had been proposed that if neutrinos had mass, then they could change from one type to another. Neutrino oscillation means that the probability of measuring a particular flavour for a neutrino varies periodically as it propagates. The first strong evidence for neutrino oscillation came in 1998 from the Super-Kamiokande collaboration in Japan, which produced observations consistent with muon-neutrinos (produced in the upper atmosphere by cosmic rays) changing into tau-neutrinos. More evidence came in 2001 from the Sudbury Neutrino Observatory (SNO), when it detected all types of neutrinos coming from the sun and was able to distinguish between electron-neutrinos and the other two flavors. Statistical analysis showed that about 35% of the arriving solar neutrinos were electron-neutrinos and the others muon or tau neutrinos. The total number of detected neutrinos agreed quite well with the earlier predictions from nuclear physics, based on the fusion reactions inside the sun. At energies above 5 MeV, solar neutrino oscillation actually takes place in the sun. So, the standard solar model was not wrong, although we still do not know the composition and processes inside the sun nor the behavior of traveling neutrinos in detail.

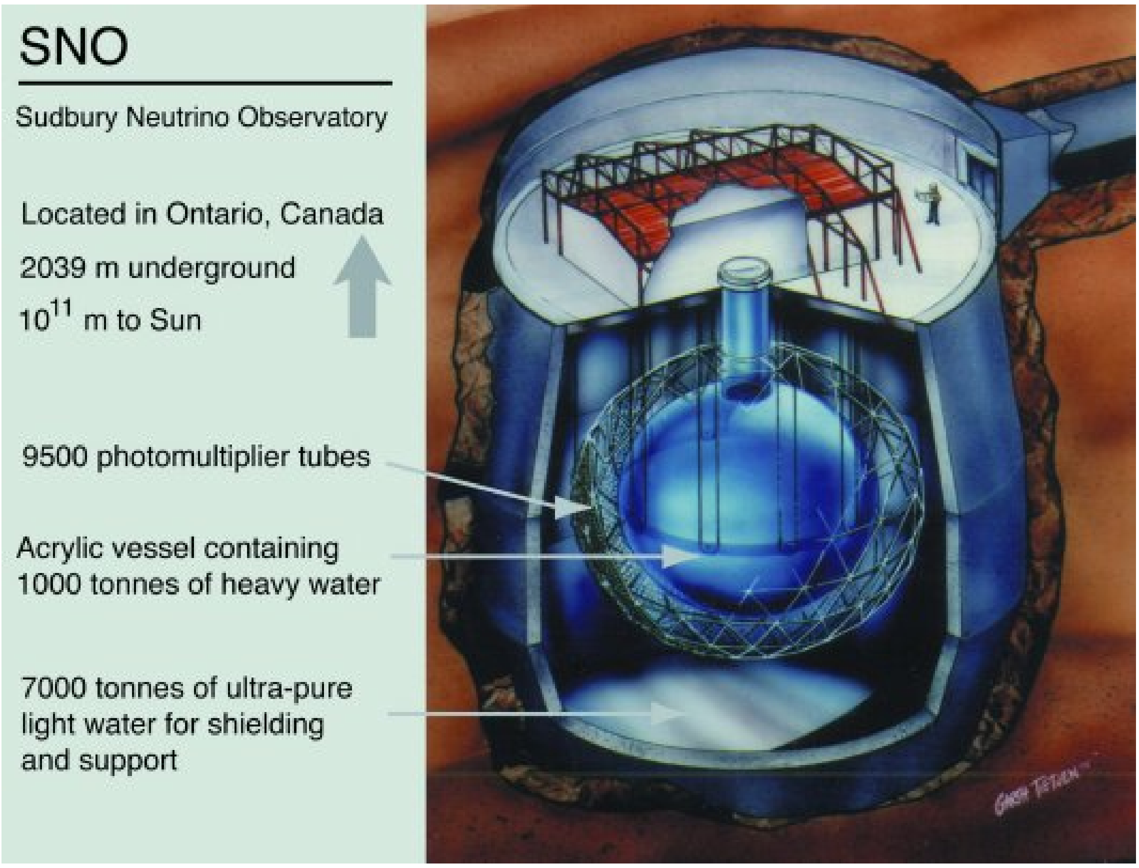


SNO was a heavy-water Cherenkov detector designed to detect neutrinos produced by fusion reactions in the sun. It used 1000 tonnes of heavy water loaned from Atomic Energy of Canada Limited (AECL), and contained by a 12 meter diameter acrylic vessel. Neutrinos reacted with the heavy water ($D_2O$) to produce flashes of light called Cherenkov radiation. This light was then detected by an array of 9600 photomultiplier tubes mounted on a geodesic support structure surrounding the heavy water vessel. The detector was immersed in light (normal) water within a 30 meter barrel-shaped cavity. Located in the deepest part of the mine, the overburden of rock shielded the detector from cosmic rays. (More details in http://nobelprize.org/nobel_prizes/physics/articles/bahcall/)

## 2.4 Sun-like stars

The results from solar physics have been used also in stellar physics. We know that stars may have 'starspots', similar to sunspots, and stellar flares, similar to solar eruptions. Hot coronae and stellar winds much like the solar wind have been predicted, although not observed yet.

The information we have of stellar objects is based on interpretations from light curves, eclipses, Doppler effects, and simulations, since the other stars are too far away to be imaged in detail. Therefore our knowledge on solar processes helps to reveal the structure and behaviour of stars in general.

# Astronomy Picture of the Day

Discover the cosmos! Each day a different image or photograph of our fascinating universe is featured, along with a brief explanation written by a professional astronomer.

2000 December 22

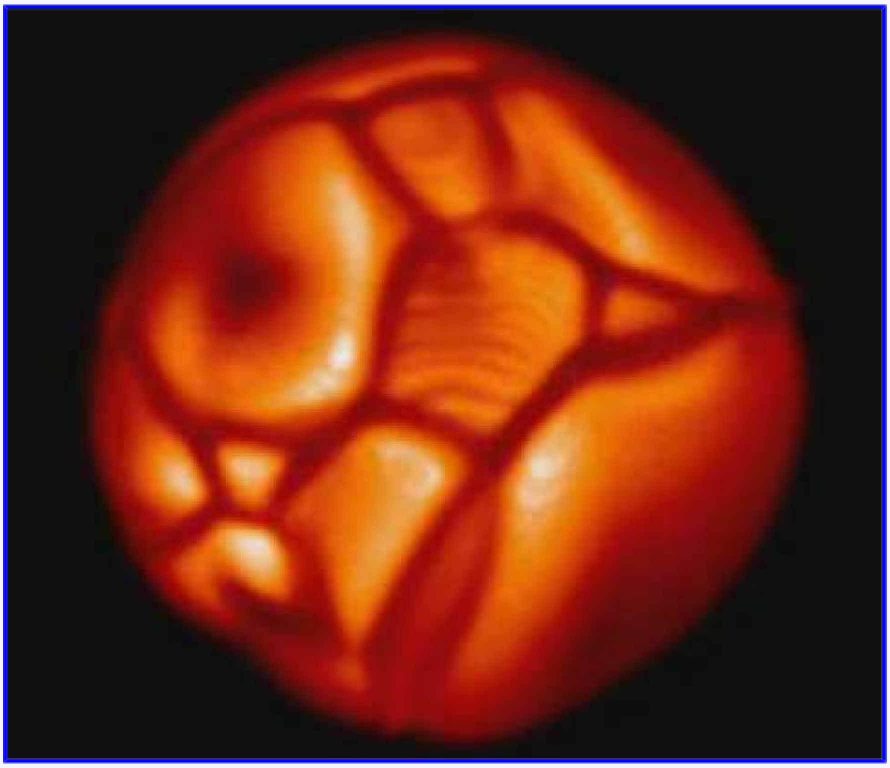

**Simulated Supergiant Star**
**Credit:** B. Freytag, (Institute for Astronomy and Space Physics, Univ. Uppsala)

**Explanation:** Looking for that perfect holiday gift for an astronomer? Consider this "star in a box". Of course, the box is actually a computational box consisting of a three dimensional grid of points, and the star is a virtual one whose physical properties and internal dynamics are numerically simulated at the points on the grid. While computers and software capable of a totally realistic numerical simulation of a complete star don't presently exist, researchers have been making progress. This picture is a movie frame from a recent numerical simulation of a supergiant star with properties intended to approximate the real star Betelgeuse. The single frame shows large convection cells and bright spots mottling the virtual supergiant's surface. Simulation movies show these surface features changing substantially with time.

# Doppler Imaging of Stellar Surface Structure

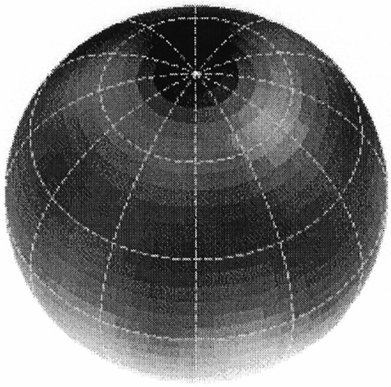

*Typical Doppler Image (HD218153 by M.Weber). That's what's possible today.*

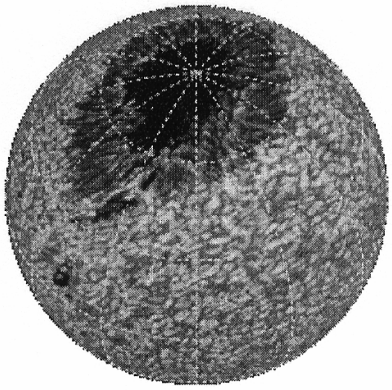

*SISP simulation (by K.Schrijver). That's what we hope for from future space interferometry. This image was composed by remapping a solar image onto a sphere.*

## Scientific Goals of this Project

One of the most challenging observational goals of today's stellar activity research is to obtain two-dimensional images of inhomogeneous stellar surfaces to relate disk integrated observations to spatially resolved surface features. Spots cooler than the undisturbed photosphere of a late-type star are a manifestation of surface magnetic fields and a time-dependent study of their latitudinal and longitudinal behavior provides a direct link to the internal stellar dynamo. Our long-term objective is thus to provide conclusive observational constraints for a generalized theory of stellar magnetism.

The near-term goal, however, is to enlarge the available sample of stars with a Doppler map and to investigate the surface spot morphology as a function of stellar rotation.

## What is Doppler imaging?

Doppler imaging is an inversion technique to recover a 2-D image of a rapidly rotating star from a series of high-resolution spectral line profiles. The inverse problem for stars with cool spots amounts to solving the integral equation relating the surface temperature distribution to the observed line profiles and light and color curve variations, while controlling the effects of noise in the data through a regularizing functional. Note that we solve for the photometric variations simultaneously with the line profiles, but that we can handle only one line per solution. If the spectroscopic phase coverage contains gaps of more than 25 degr on the stellar surface more weight is shifted to the photometry. In a recent application to the K-dwarf LQ Hya (Strassmeier, Rice, Wehlau et al. 1993, A&A 268, 671) we made up an average map from nine spectral lines and two broad-band colors. This ensured that spurious features from a single line, caused by noise or any other systematic error, will be suppressed in the final map.

## Optical, Ultraviolet, and X-ray Observations Planned and in Progress

# Mapping starspots and magnetic fields on cool stars

***Andrew Collier Cameron,Ron Hilditch, Moira Jardine and David James, Tim Lister, Sandra Jeffers***

**Recent highlights:**

- **2001: AB Dor does the twist!** Differential rotation discovered to be changing with time.
- **1997: First measurement of differential rotation** on a star other than the Sun.
- For images illustrating these highlights, go to the AB Dor Picture Gallery

The cool stars group at St Andrews uses indirect imaging methods, including Doppler tomography, Zeeman-Doppler imaging, eclipse mapping and prominence tomography to make maps of cool starspots and other magnetic structures on and above the surfaces of rapidly rotating stars. With Jean-Francois Donati (Toulouse) and Meir Semel (Meudon) we have established a world-leading long-term programme of Zeeman-Doppler imaging at the Anglo-Australian Telescope. This enables us to map changes in magnetic-field patterns on stellar surfaces from year to year. This programme also produced the first detailed measurements of surface differential rotation on stars other than the Sun, by enabling us to use starspots as tracers of large-scale fluid shear. We find that even in stars rotating 50 times faster than the Sun, the differential rotation rate is similar. We are using these powerful new observations to extend what we know about physics of similar structures on the Sun (spots, prominences, etc) to the much more densely-packed magnetic structures we see on other, more active stars. We now suspect that 40% or more of some starsí surfaces are covered in dark magnetic spots, and we are developing sensitive new eclipse-mapping methods to determine the packing fraction and size distribution of these structures.

## How Doppler imaging works:

The term ''Doppler imaging'' was coined by Vogt & Penrod (1983), who demonstrated that travelling starspot bumps were observable in the line profiles of HR 1099, and that an image of the stellar surface could be derived from them. A photospheric absorption line in which rotation is the dominant broadening mechanism displays time-variable irregularities if the visible surface of the star is mottled by dark spots. The effect of a cool, dark region on a rotationally-broadened line profile is illustrated in Fig. 1.

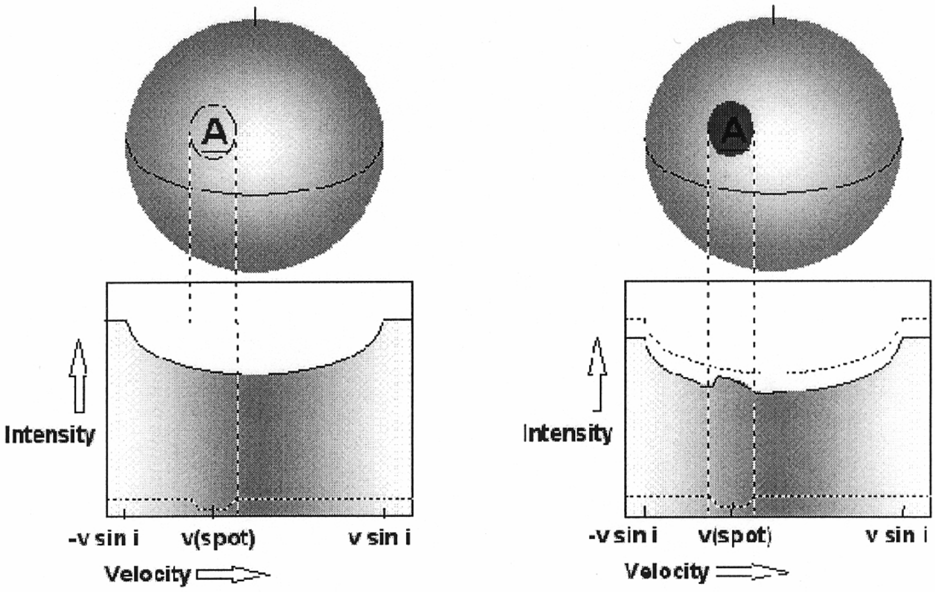


**Fig. 1:** The ''missing'' light of the spot consists of a continuum contribution that spans the line profile, plus a narrow line contribution that is Doppler shifted by an amount that depends on the projected distance of the spot from the stellar rotation axis. Removing this light causes an overall depression of the continuum, but less light is removed at the Doppler shift of the spot relative to the centre of the line. The observable signature of a dark spot on the stellar surface is therefore a bright bump in every photospheric absorption line in the star's spectrum.

As the star rotates, the spots are carried across the stellar disc, causing the bumps to change their Doppler shifts in accordance with their projected distances from the star's rotation axis. Spots near the equator remain visible for half the stellar rotation cycle, tracing out a sinusoidal velocity variation with an amplitude equal to the stellar equatorial rotation velocity, Vsini. Spots at progressively higher latitudes follow progressively lower-amplitude sinusoids. The fraction of the rotation cycle for which a spot remains visible depends on its latitude and the inclination of the stellar rotation axis to the line of sight. The times at which spot signatures cross the centre of the line profile thus reveal their longitudes, while the amplitudes of their sinusoids (or equivalently, their radial accelerations at line centre) tell us their latitudes.

For a fuller account of the technical details and recent results, the following resources are available:

- Slides from review talk given at International Workshop on Astro-tomography, Brussels (July 2000)
- Review paper to appear in proceedings of Brussels workshop

## Zeeman-Doppler imaging

This is a variant on the Doppler imaging technique. It uses circular and linear polarization information to measure the small shifts in wavelength and profile shape that arise in the presence of a magnetic field. Both the strength of the field and its orientation relative to the line of sight can be determined. As in conventional Doppler imaging, the rotation of the star is used to resolve different magnetic regions on the stellar surface. Jean-Francois Donati has an excellent web page describing this technique.

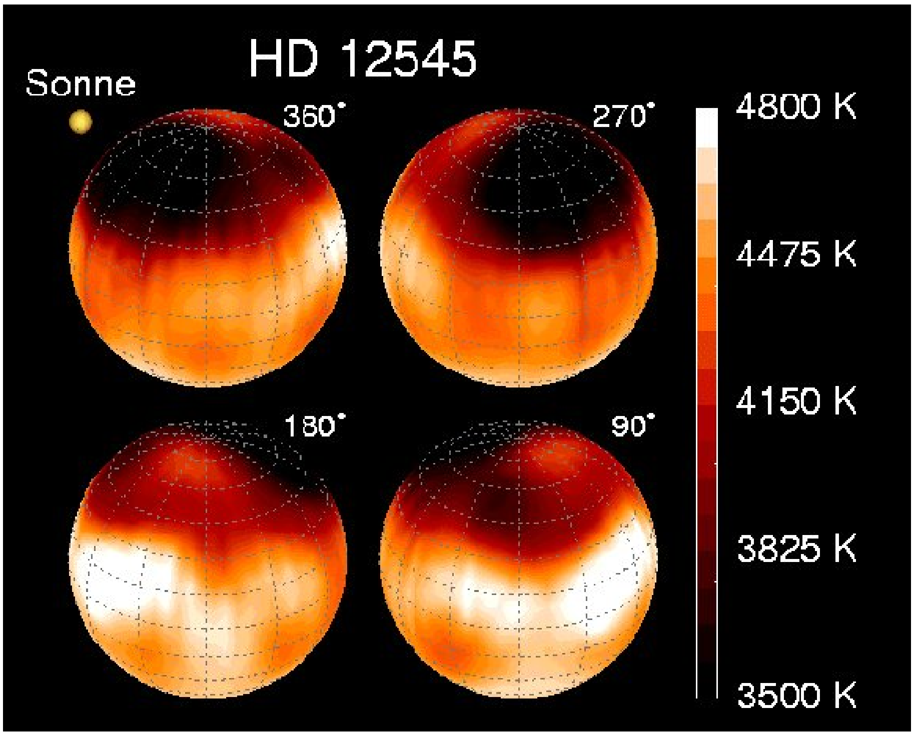


Figure 2.5: Doppler images of the giant star HD 12545 (= XX Triangulum) and its super starspot. It is a K0 giant star, a cool star that is approximately ten times larger and two times more massive than the Sun. In order to observe spots on the surfaces of other stars, astronomers need to "resolve" the stellar disk. This cannot be done with even the largest (existing and planned) telescopes but here the researchers applied an indirect imaging technique called Doppler imaging. The star was observed for 24 consecutive (clear) nights, to cover the whole stellar rotation period. The color coding in the image is proportional to temperature. Dark means cooler than the effective temperature and white means hotter. An image of the solar disk is shown to scale as a comparison. Surprisingly, HD 12545 had a warm spot (350 K above photospheric temperature; the white area in the picture) on the hemisphere adjacent to the cool super spot. It is speculated that the warm spot harbors the same magnetic field as the cool spot but being of opposite polarity. (Text from the press release of a paper by Strassmeier, A&A, 347, 225, 1999.)

For more on this topic, see for example A. Collier Cameron: Spot Mapping in Cool Stars. Lecture Notes in Physics, Vol. 573, s. 183-206, 2001.

Doppler image gallery is available at
http://www.aip.de/groups/activity/DI/maps/

See Doppler imaging movie at Svetlana Berdyugina's website, Starspots and Stellar cycles,
http://www3.kis.uni-freiburg.de/~sveta/Starspots/starspots.html

## Flare Stars

Many of the flare stars are dim, red (class-M) dwarfs that exhibit unusually violent flare activity. A solar-flare-sized flare occurring on Proxima Centauri would emit about as much light as Proxima Centauri itself. From our standpoint here on the Earth, it would appear that, during the flare, Proxima Centauri doubled in brightness. Flares on flare stars occur sporadically, with successive flares spaced anywhere from an hour to a few days apart. Flares on such dim dwarfs may emit up to 10 000 times as many X-rays as a comparably sized flare on our own sun. They would be lethal to any life forms otherwise developing on planets near the flare star, so life around such stars is unlikely. (Even if life could spring up despite the flares, flare stars are red dwarfs anyway, meaning that they have very narrow comfort zones due to their dimness and may be too red in color for plants to perform photosynthesis.) Some flare stars have also been observed emitting radio bursts simultaneously with the flares.

Note that since flare stars are variable stars, they will usually have a variable star designation such as UV Ceti or V645 Centauri. As more and more red dwarfs are observed in detail, more and more of them are being classified as flare stars. It may turn out that most red dwarfs are flare stars, and that red dwarfs without violent flare activity are the exception rather than the rule. Some of the flare stars included in this compendium are: UV Ceti, Alpha Centauri Proxima, Wolf 359, and FL Virginis.
(Text from `http://www.stellar-database.com/`

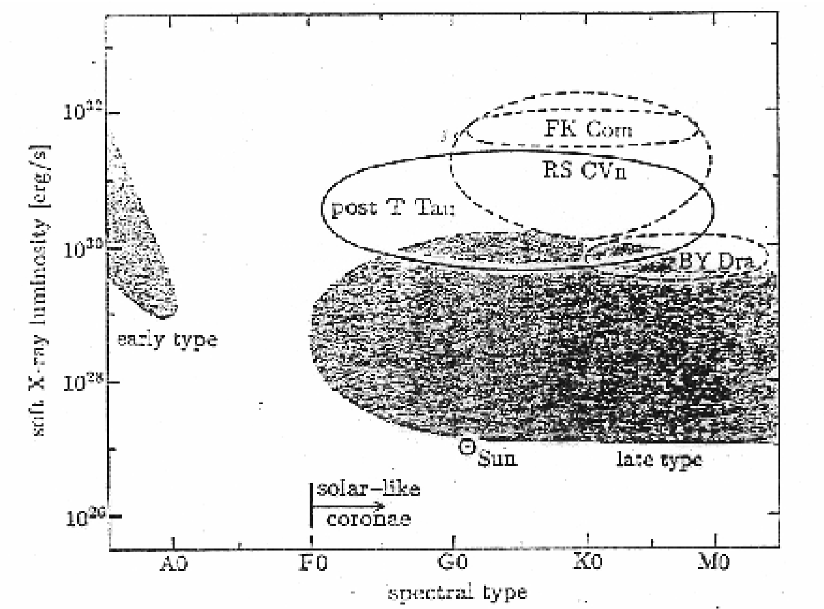


O...B stars: hot stellar winds F...M stars: hot corona

Conditions for the solar–type corona:
- convection layer below the photosphere
- stellar rotation (the faster, the larger luminosity)

Studied stars:
Proxima Centauri (nearest star to the Sun, M5.5, flares, red dwarf)
AB Doradus (K1, starspots(?), fast–rotating orange dwarf)

## 2.5 Helioseismology

# Helio- and Asteroseismology

INTRODUCTION | OBSERVATIONS : the SUN | OBSERVATIONS : STARS | MODELS | SOLAR OSCILLATIONS | RESULTS
WHO ARE WE ?

## Solar oscillations

The oscillations in the Sun are sound waves, generated by the convection much like a guitar is played by plucking the strings.

If we follow where a sound wave goes, starting from the surface, it first moves into the Sun almost straight towards the centre. Its path then slowly bends around, because of the increasing sound speed, so that it misses the centre of the Sun. How exactly it moves therefore depends on the details of the sound speed inside the Sun. The point of closest approach is known as the *turning point* of the mode. After the turning point the wave moves out again until it reaches the surface. At the surface it is reflected as if by a mirror and it goes back in again.

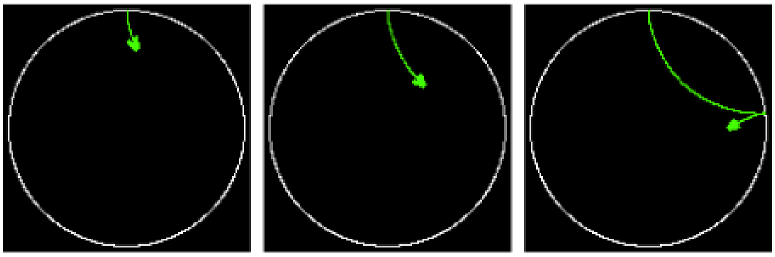

Here are a few examples of how sound waves propagate into the Sun, with some animated sequences.

These sound waves give rise to so-called *standing waves*, in the same way that a vibrating string shows standing waves. In the Sun we are talking about standing waves in three dimensions of course. Here we show some examples of how the waves look on the solar surface (the amplitude is very much enhanced).

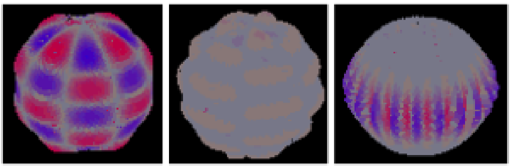

This page contains more information about oscillations on the solar surface.

The oscillation pattern on the surface can be characterised by node lines, on which the motion vanishes. The total number of node lines is called the degree $l$. The oscillation modes can also have node lines at constant longitude. There are a number $m$ of those which is always less than or equal to the degree $l$. Inside the Sun the amplitude of the standing waves can have a number $n$, called the radial order of the mode, of nodes at certain radii from the centre.

# HELIOSEISMOLOGY

- p modes (outer layers)
- g modes (core)
- f modes (surface gravity waves)

## Observations

- 5 minute p modes
- 160 min oscillation (?)
- 13 day oscillation

etc.

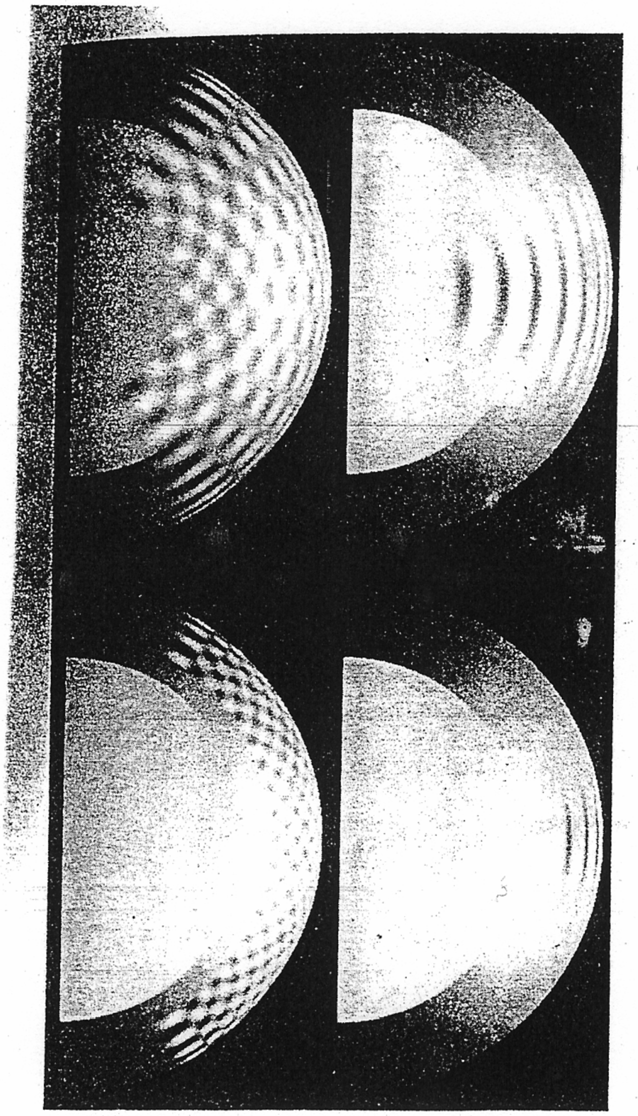

$l=20$ (spherical harmonic degree)

$l=60$

Figure 3. Superimposed on the model of Figure 2 are oscillation patterns arising from p modes with frequencies of about 3 mHz. These plots show the rough extent in depth and latitude of modes of $l$=20 (top) and 60 (bottom). The left column shows modes with $m$ values = $l$/2 and the right column shows sectoral modes.

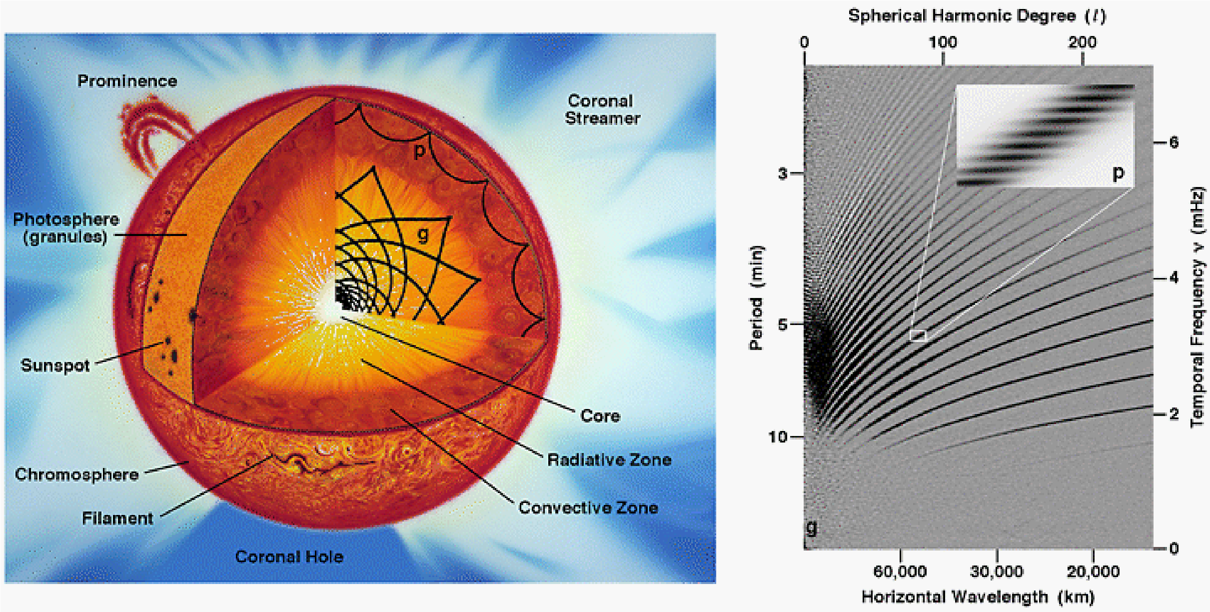
Prominence
Coronal Streamer
Photosphere (granules)
Sunspot
Chromosphere
Filament
Coronal Hole
Core
Radiative Zone
Convective Zone
p
g
Spherical Harmonic Degree (l)
0
100
200
Period (min)
3
5
10
Temporal Frequency ν (mHz)
6
4
2
0
60,000
30,000
20,000
Horizontal Wavelength (km)

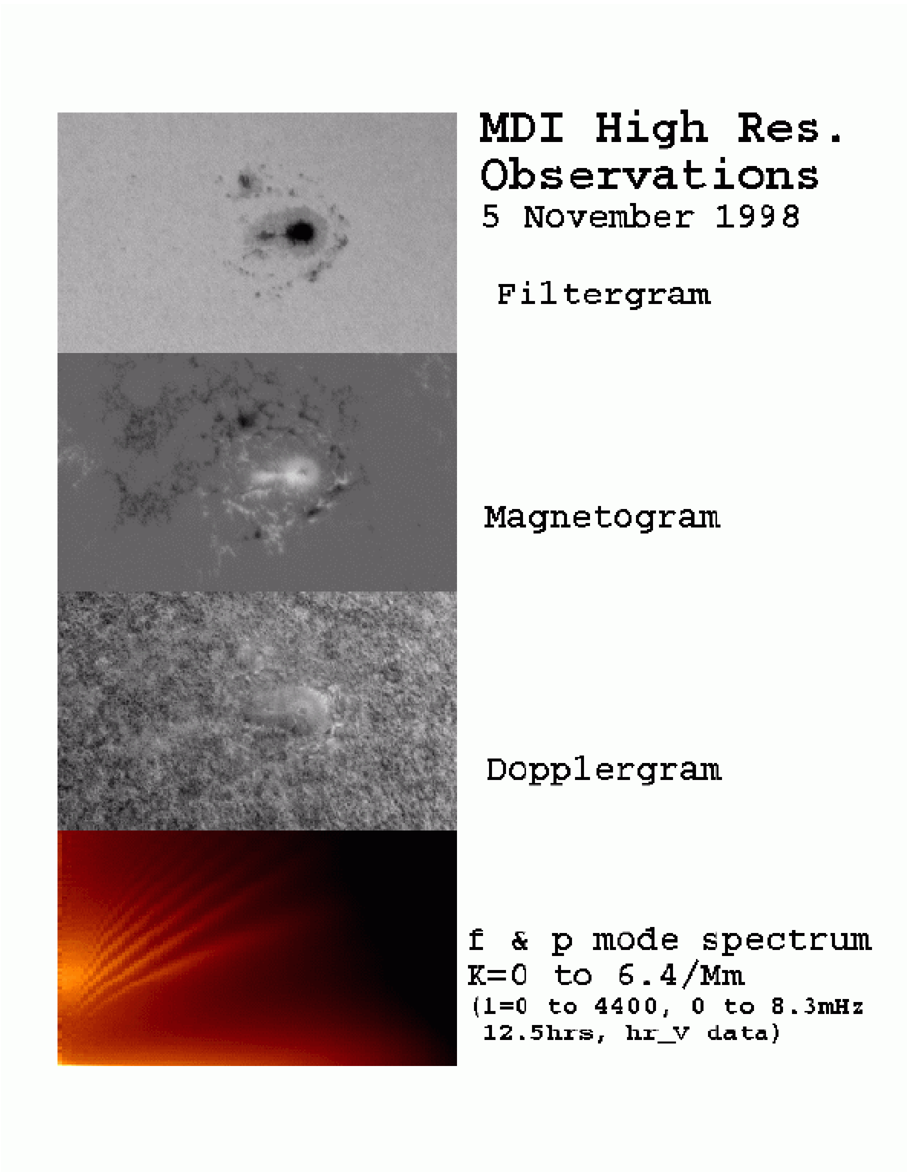
MDI High Res. Observations
5 November 1998
Filtergram
Magnetogram
Dopplergram
f & p mode spectrum
K=0 to 6.4/Mm
(l=0 to 4400, 0 to 8.3mHz
12.5hrs, hr_V data)

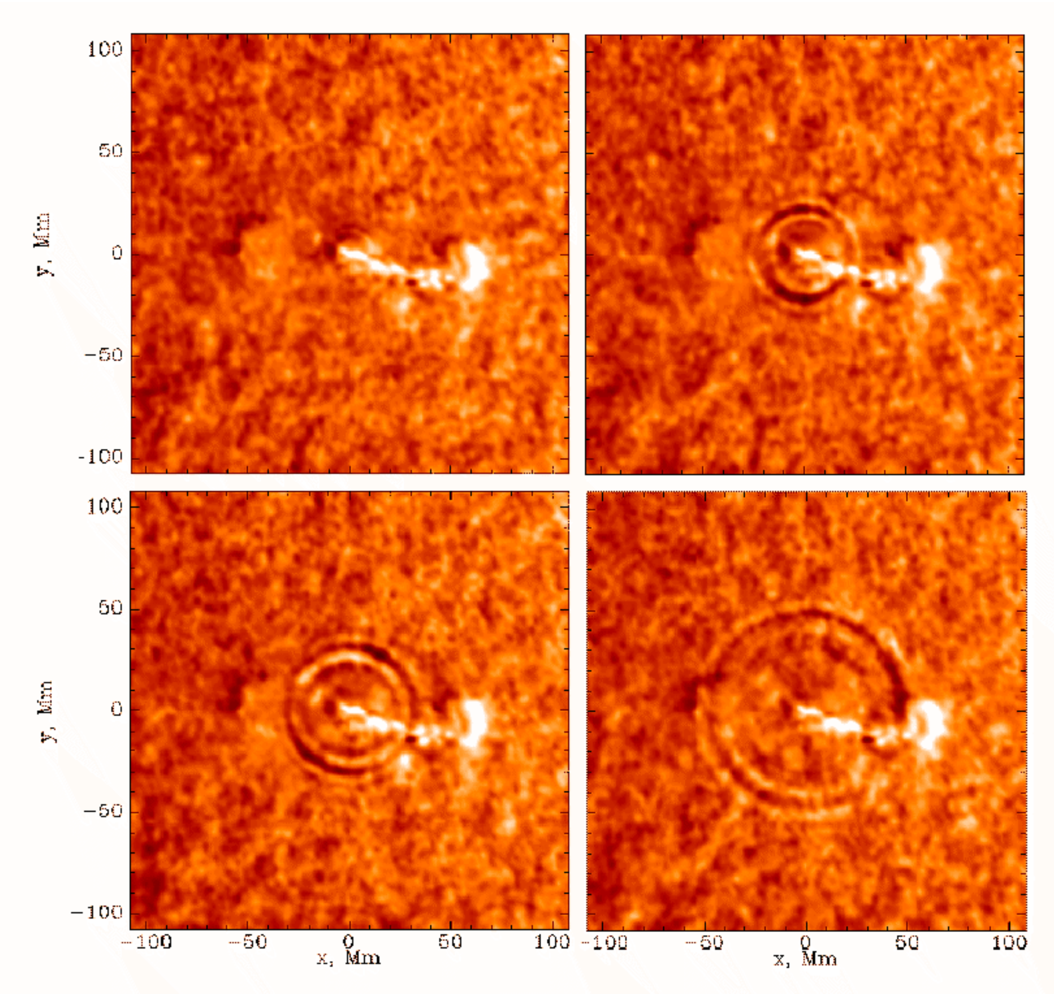


Scientists have shown for the first time that solar flares produce seismic waves in the Sun's interior that closely resemble those created by earthquakes on our planet. The researchers observed a flare-generated solar quake that contained about 40,000 times the energy released in the great earthquake that devastated San Francisco in 1906. The amount of energy released was enough to power the United States for 20 years at its current level of consumption, and was equivalent to an 11.3 magnitude earthquake, scientists calculated.

The solar seismic waves appear to be compression waves like the "P" waves generated by an earthquake. They travel throughout the Sun's interior. The solar quake that the science team recorded looks much like ripples spreading from a rock dropped into a pool of water. But over the course of an hour, the solar waves traveled for a distance equal to 10 Earth diameters before fading into the fiery background of the Sun's photosphere. Unlike water ripples that travel outward at a constant velocity, the solar waves accelerated from an initial speed of 22,000 miles per hour to a maximum of 250,000 miles per hour before disappearing.

Images were taken with the Michelson Doppler Imager (MDI) onboard the Solar and Heliospheric Observatory (SOHO) spacecraft, immediately following a moderate-sized flare on July 9, 1996 (reported at the Conference of the American Geophysical Union, 27 May 1998).

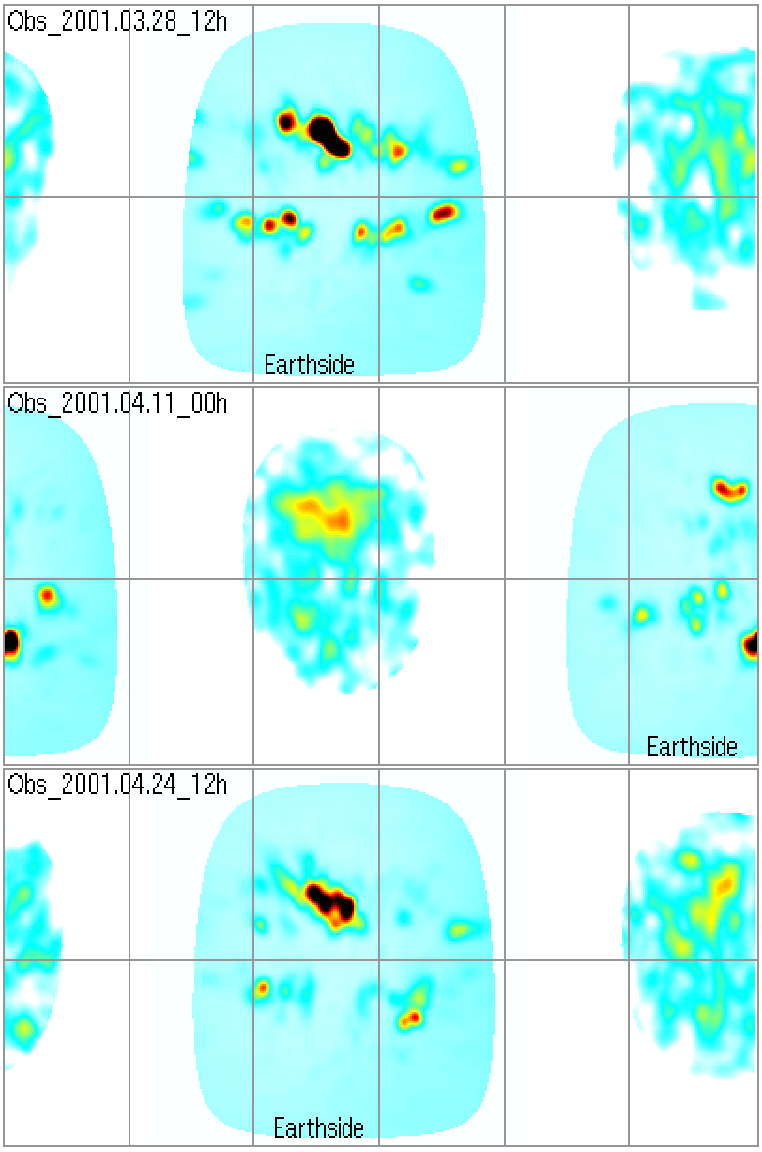


Figure 2.6: In March 2000 the SOHO/MDI science team announced the first images of an active region on the far side of the Sun. Since mid-2001 these far side images of the central area of the back side of the Sun have been prepared for each 12-hours and made available on the web. Since the Sun rotates on its axis in about 27 days, regions facing the Earth rotate off the visible surface after at most 13 days. They can emerge at any longitude, surprising solar observers if they form on the back side of the Sun and rotate into view as already very active centers. The method is using the travel time of sound waves which are bounced from the underside of the surface (Earth-side) going to and coming from each location on the farside (back-side). Because the sound speed beneath active regions is a bit faster than other places and because the reflecting layer beneath active regions is a bit deeper than other places, waves that include an active region at one of their bounce places will return to the front side a bit sooner than other waves. To make these backside images, surface motion maps are taken each minute and each map contains about 30 000 measurements. The computation for each farside map takes about 2.5 hours on a fast computer. (Text and more details in, e.g., http://soi.stanford.edu/press/farside_Feb2006/web/)

## 2.6 Solar magnetic fields

Magnetic fields play a dominant role in solar activity. Solar eruptions are powered by the energy stored in the magnetic fields, and to understand what triggers the eruptions, we have to know first where the energy comes from. Observations show how magnetic fields are raised from the solar interior to the sun's surface, but the primary energy release happens high in the chromosphere and corona.

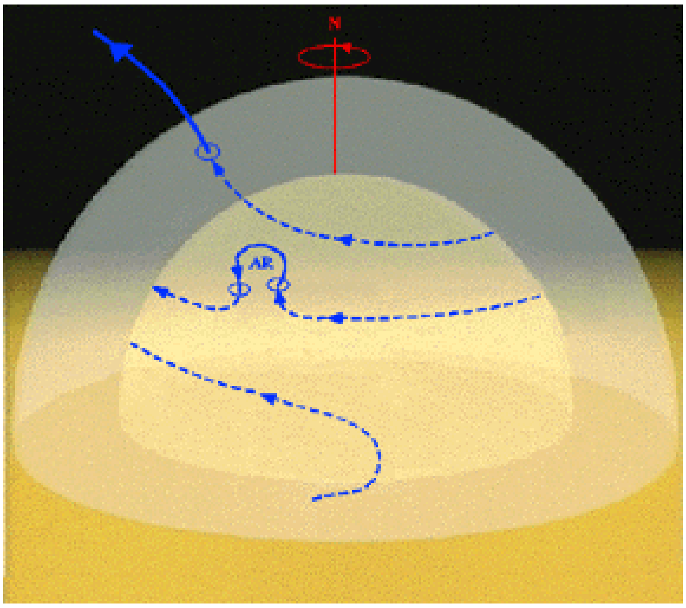


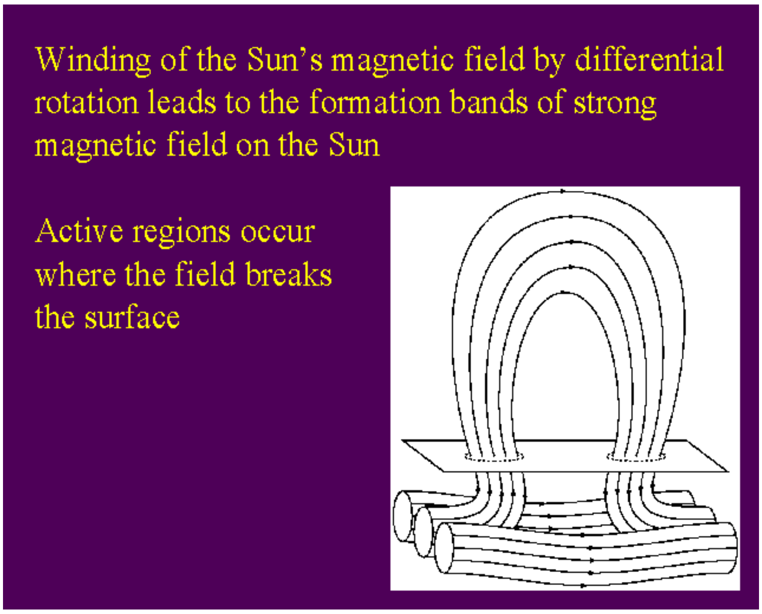

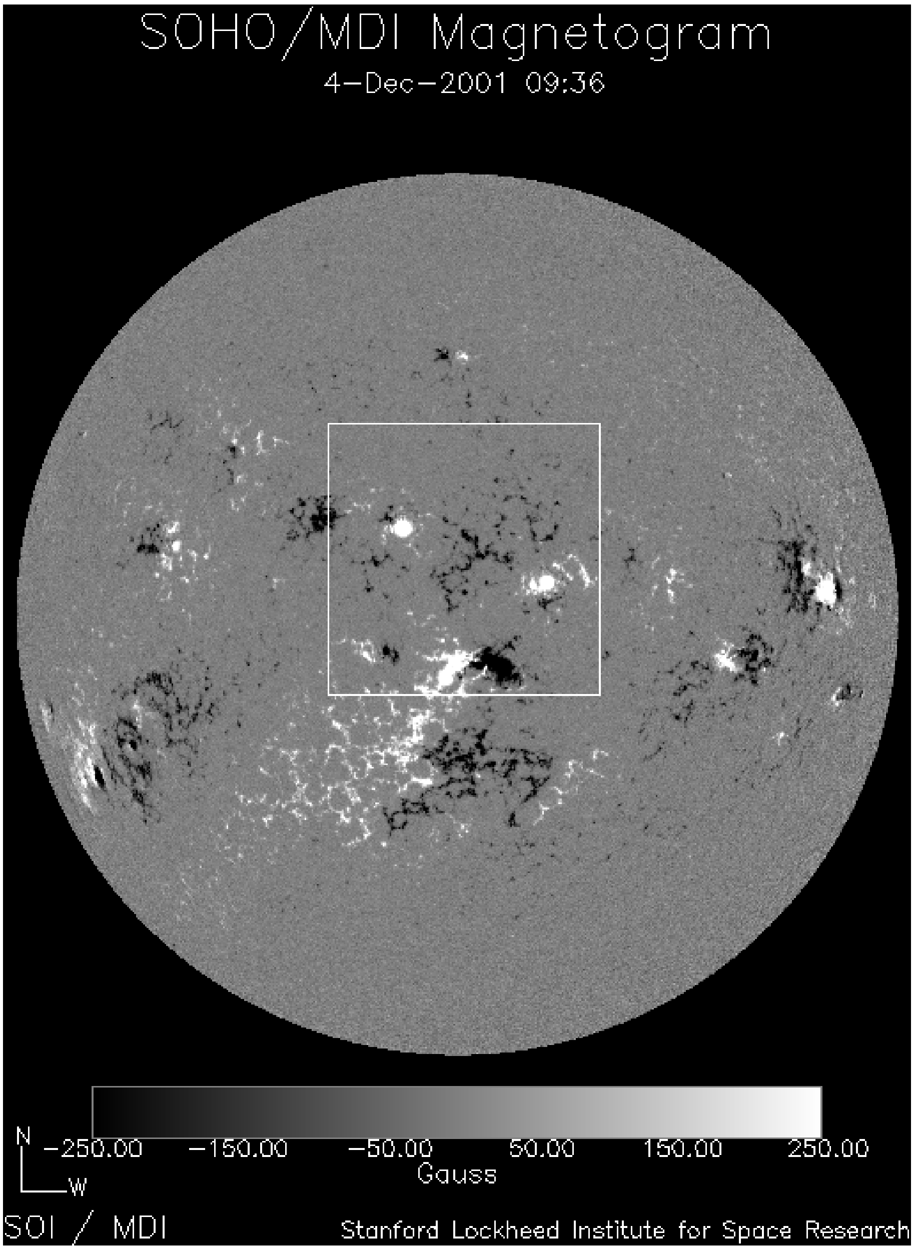


Figure 2.7: A magnetogram from SOHO MDI shows the photospheric fields between -250 and +250 Gauss. Within the active regions the field strength can be as high as 2000 – 3000 G. Magnetic field observations are done using the Zeeman splitting of photospheric spectral lines.

One scenario – although the idea is not supported much these days – is that when the sun was formed by contraction of a gas cloud, a 'primordial' magnetic field was dragged in, and that the interior still holds this relic field. In support to this model, researchers have found 'active longitudes' (i.e., longitudes where repeated activity is observed) that could be a sign of the relic fields.

However, it is now widely accepted that the field regenerates itself continuously, and to do this a dynamo mechanism is needed. A dynamo converts kinetic energy of an electrically conducting body (like the plasma inside the sun, in motion because of convection, for example) into magnetic energy. It has been found that a 'seed' magnetic field can form much larger fields if certain motions are present. These fields can also oscillate, with periods that possibly explain the 22-year solar magnetic cycle and the 11-year activity cycle.

There are many models that try to explain where and how the dynamo works. One basic thing that needs to be explained is the switching between the poloidal and toroidal field (i.e., how to generate fields that are first parallel to lines of longitude, then change into fields parallel to latitude, and then regenerate back the fields that are parallel to longitude). The migration of sunspots and the formation of the butterfly diagram is part of this problem.

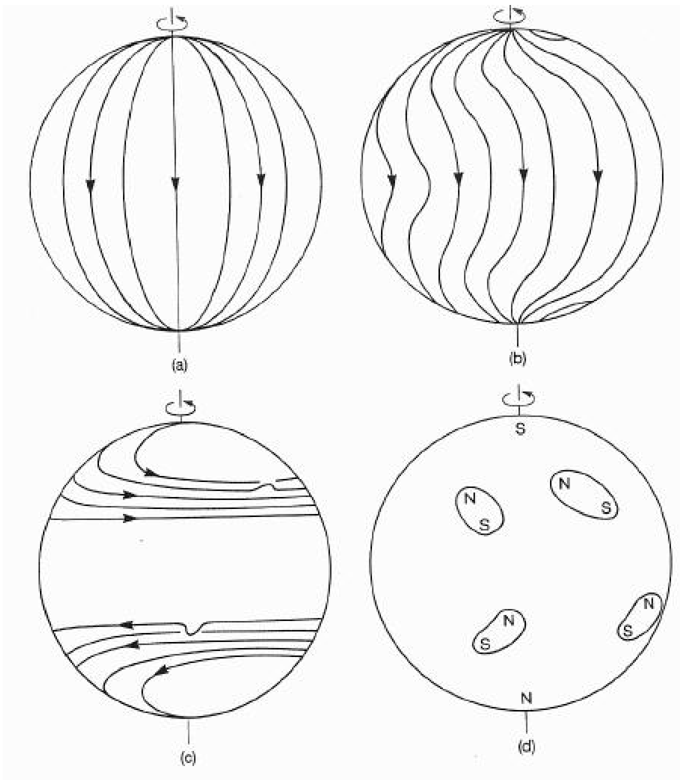


Figure 2.8: Simplified scheme for the generation of sunspot magnetic fields; the first model was developed by H.W. Babcock in 1961. The scheme shows how the entirely poloidal field (a) is deformed by differential rotation (b,c), and the active regions with bipolar sunspot groups get formed (d). Sunspot migration then neutralizes the field, and the poloidal field is regenerated – but now with opposite polarity sunspots. This explains the full 22-year magnetic cycle. (From K.J.H. Phillips: Guide to the Sun, Cambridge University Press, 1992)

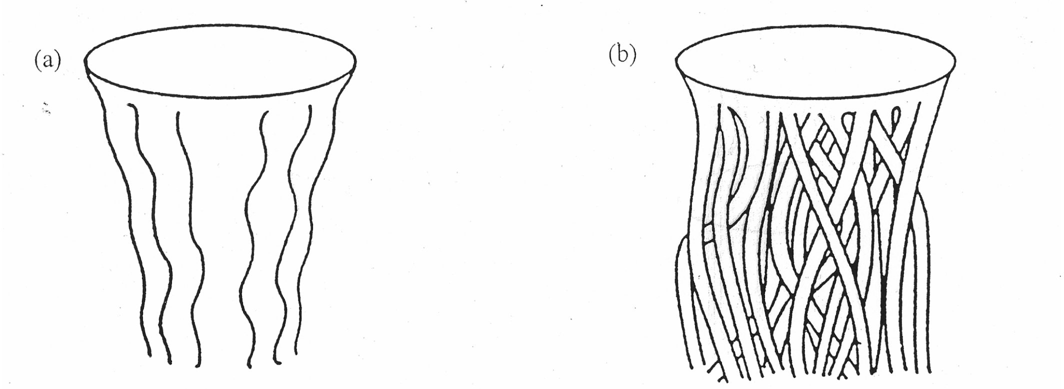


**Fig. 37.** Two possible magnetic field behaviours below a sunspot. (a) coherent flux tube and (b) tight cluster (diagram courtesy of Thomas, J H and Weiss, N O).

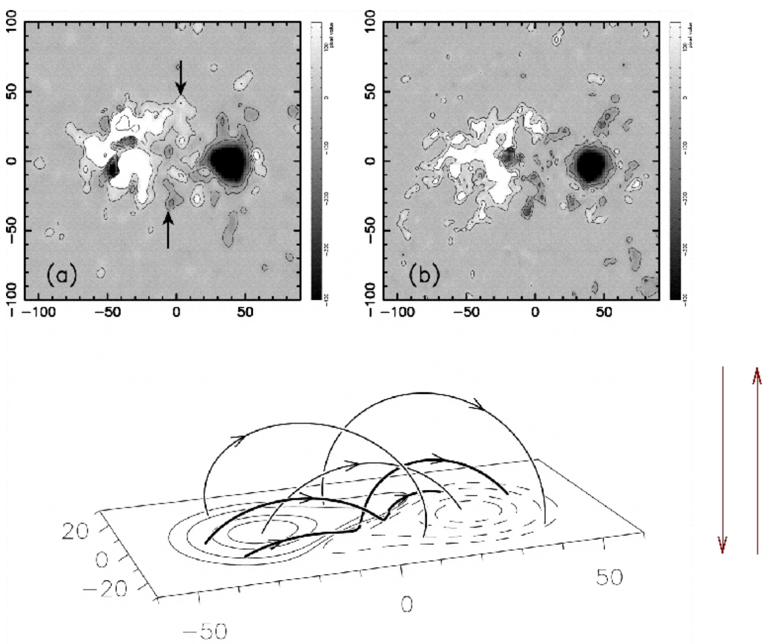


Figure 2.9: Magnetic flux is measured along the line-of-sight, and twisted fields are observed only in projection. When the flux tube is twisted, an asymmetry appears in the magnetogram because of the contribution of the azimuthal component to the observed vertical component of the field. The vertical projection of the azimuthal component produces two elongated polarities ("tongues"), which extend between the main ones. The strength of these tongues is directly proportional to the magnitude of the twist and their position depends on the sign of the twist. (Image and part of the text from Lopez Fuentes et al. ApJ 544, p. 540-549, 2000.)

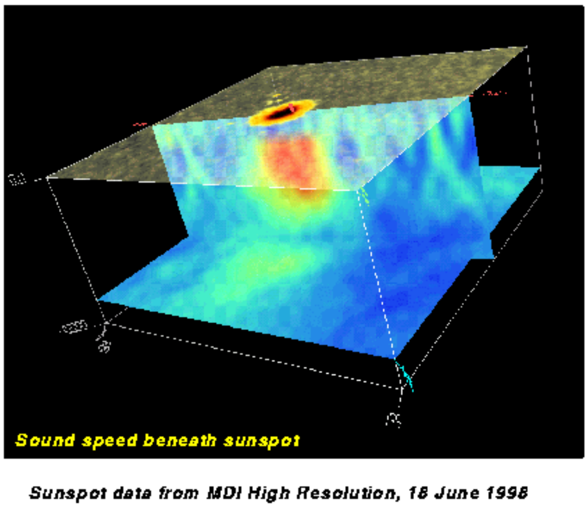


Figure 2.10: An image of the sound speed below a sunspot derived from dopplergrams observed with the Michelson Doppler Imager onboard the Solar and Heliospheric Observatory spacecraft using the technique of time-distance helioseismology. Three planes are shown, on top the intensity at the surface which shows the sunspot with the dark central umbra surrounded by the somewhat brighter, filamentary penumbra. The second plane is a vertical cut from the surface to a depth of 24000 km showing areas of faster sound speed as reddish colors and slower sound speed as bluish colors. The sound speed is affected both by the temperature of the gas and the magnetic field, which we know to be strong in the sunspot at the surface. The normal increase of sound speed with depth in the sun has been subtracted so that we are only looking at deviations from the average. The third plane (bottom) is a horizontal cut at a depth of 22000 km showing the horizontal variation of sound speed over a region of 150000x150000 km.

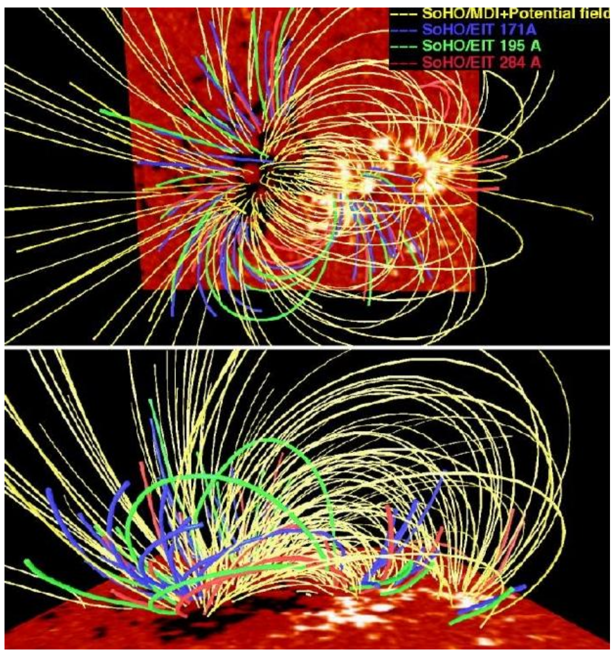


Figure 2.11: 3-D simulation of an active region (Aschwanden et al., 2000).

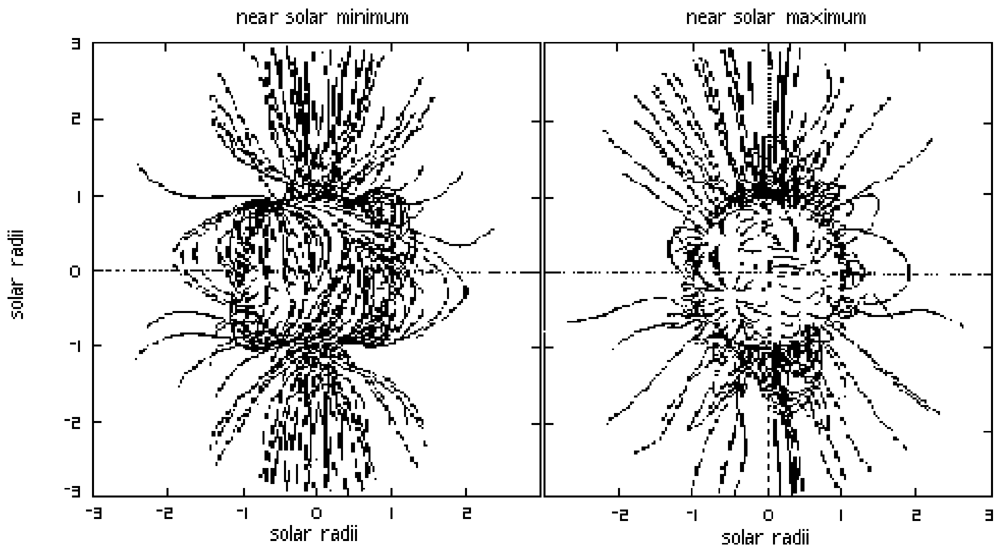


Figure 2.12: Solar magnetic field during activity minimum and maximum.

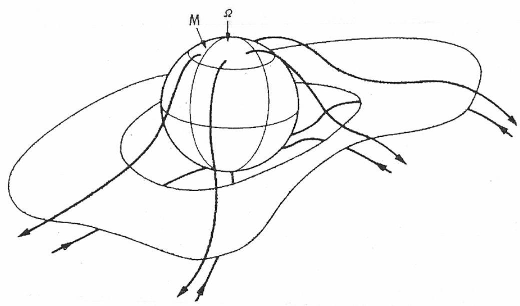


**Fig. 8.11.** Current sheet in the inner heliosphere in the Ballerina model. The thick lines indicate the magnetic field lines. Reprinted from Smith et al. [8.82], *J. Geophys. Res.* **83**, Copyright 1978, American Geophysical Union

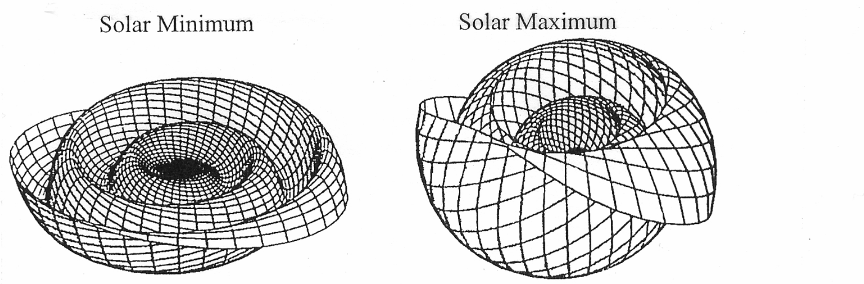


**Fig. 8.20.** Waviness of the heliospheric current sheet during solar minimum and maximum conditions, based on a sketch by R. Jokipii, University of Arizona

Figure 2.13: Solar magnetic field is often described as the 'ballerina skirt'. The skirt looks different during activity minimum and maximum.

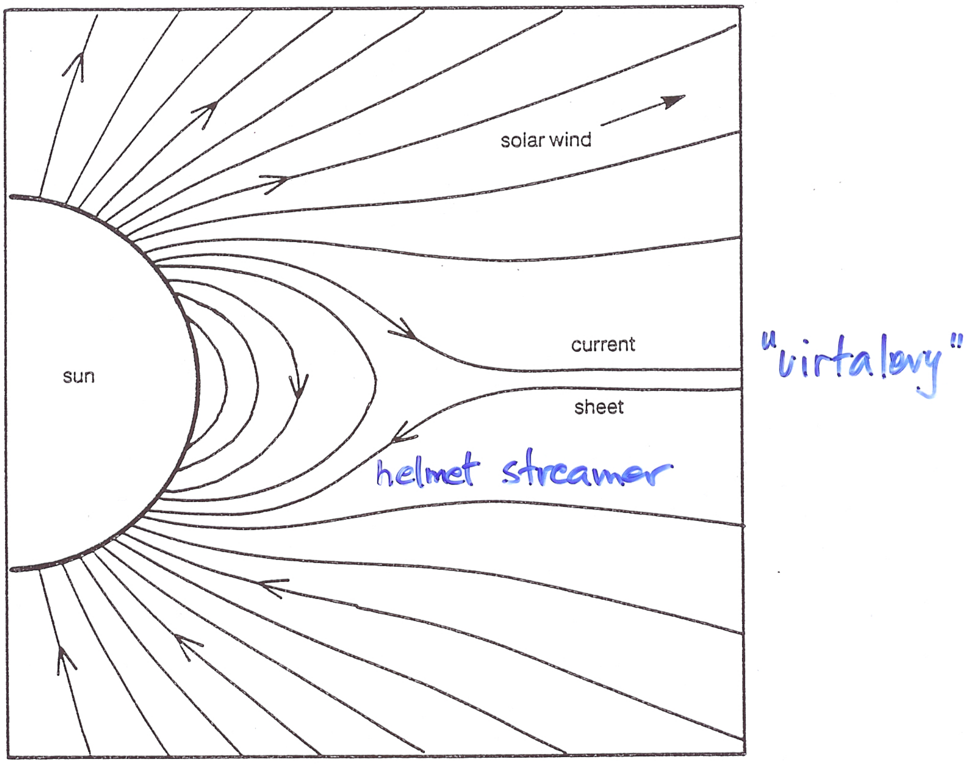


Fig. 5.15 Calculated magnetic field configuration at the time of solar minimum: a dipolar field stretched out by the solar wind to form a helmet structure near the equator and a current sheet. (After Pneuman and Kopp (1971). Reprinted by permission of Kluwer Academic Publishers)

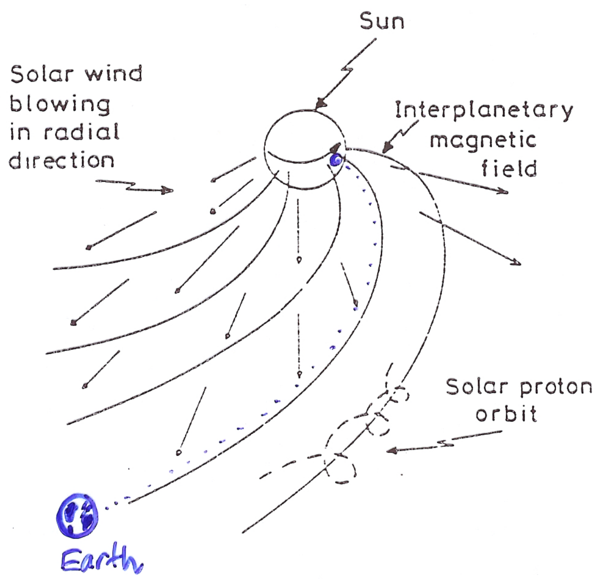


Figure 2.14: Some solar longitudes are "well-connected" to the Earth (~ W70 – 80).

## 2.7 Hale's and Joy's laws

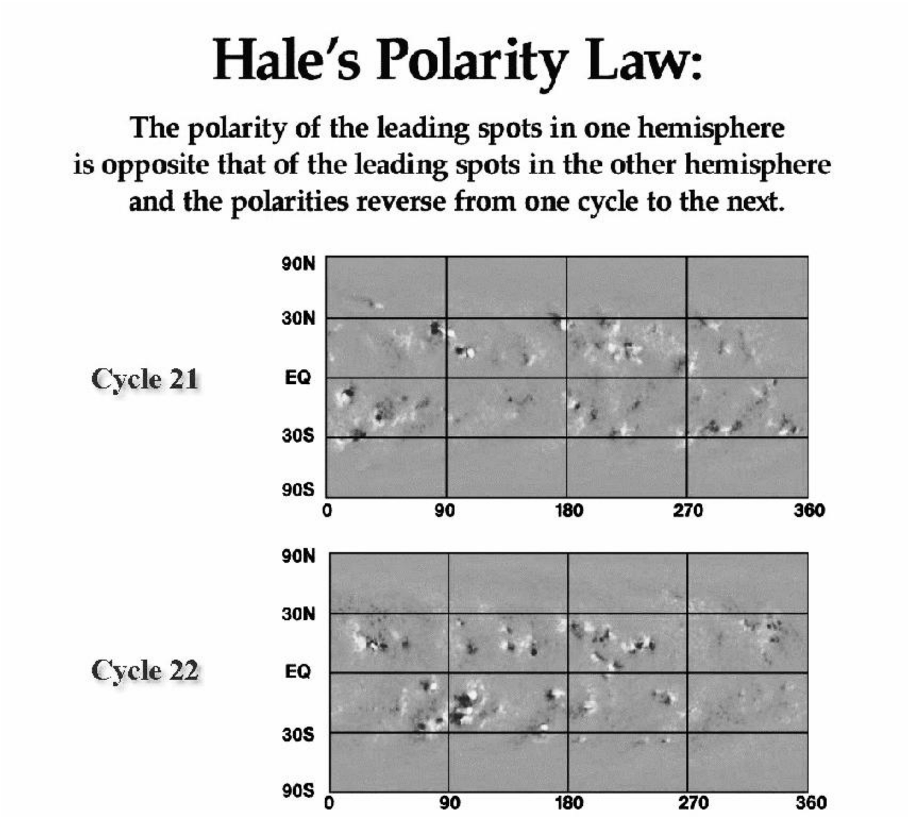


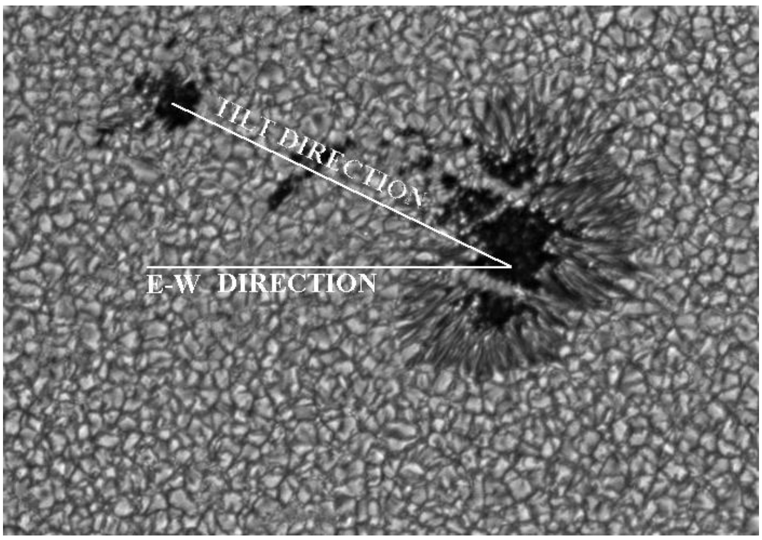


Figure 2.15: Joy's law: The magnetic axis of the sunspot group is usually slightly inclined to the solar east-west line, running from 3 degrees near the equator to 11 degrees at latitude 30 N/S, with the preceding polarity spot being slightly closer to the equator. If the axis is highly tilted initially, the group will tend to rotate until the axis is more parallel to the equator.

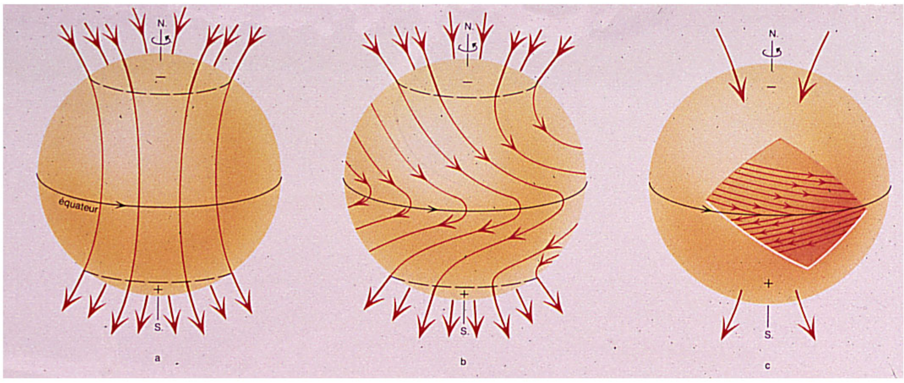


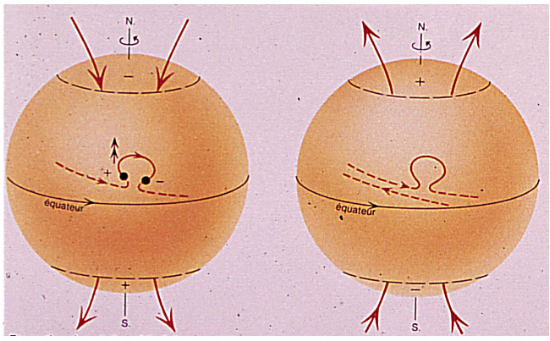


## 2.8 Differential rotation

Magnetic fields within the Sun are stretched out and wound around the Sun by differential rotation - the change in rotation rate as a function of latitude and radius within the Sun. This is called the *omega-effect* after the Greek letter used to represent rotation. Twisting of the magnetic field lines is caused by the effects of the Sun's rotation. This is called the *alpha-effect* after the Greek letter that looks like a twisted loop (see schematic drawings at http://solarscience.msfc.nasa.gov/dynamo.shtml). Recent dynamo models assume that the twisting is due to the effect of the Sun's rotation on the rising magnetic field flux tubes. The twist produced by the alpha effect makes sunspot groups that obey Joy's law and also makes the magnetic field reverse from one sunspot cycle to the next (Hale's law). But, there is differential rotation also *inside* the sun.

The sidereal rotation rate Ω (degrees/day) can be expressed as

$$\Omega = A + B \sin^2 \theta + C \sin^4 \theta \tag{2.5}$$

where $\theta$ is the solar latitude in degrees, and $A$, $B$ and $C$ are the fitted constants.

*Sidereal* (true) rotation rate is calculated from the observed, *synodic*, rotation rate by correcting for Earth rotation.

Surface rotation rates can be calculated using relatively stable features like sunspots, quiescent filaments and radio bright regions. First, solar images must be made comparable by rotating the images so that North is up and West is to the right. This is called correcting for the P angle. Correction for the $B_0$ angle is more demanding, and it is usually done by superposing a grid on the disk (after fitting the solar limb). After the corrections, the latitude and longitude values of each feature can be recorded and followed at suitable intervals. It should be noted that for example sunspots tend to disintegrate and/or merge together, so the time between observations should not be too long.

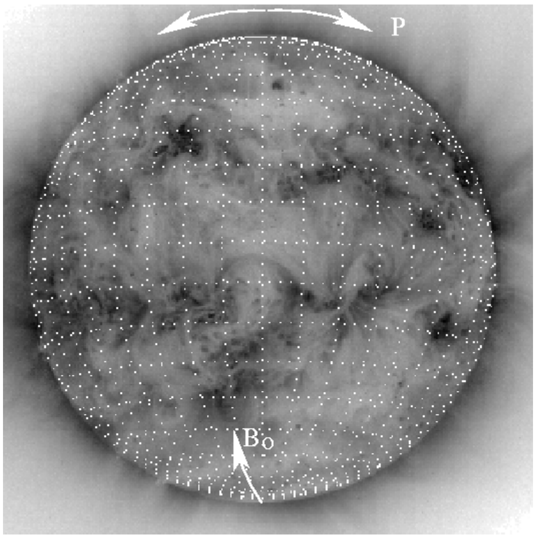


Figure 2.16: The sun at 195 Å:n observed in February 2000. Grid separation is 10 degrees and the value of $B_0$ is -6 degrees, which means that the south pole is tilted towards us. North is up (a correction for the P angle has been made).

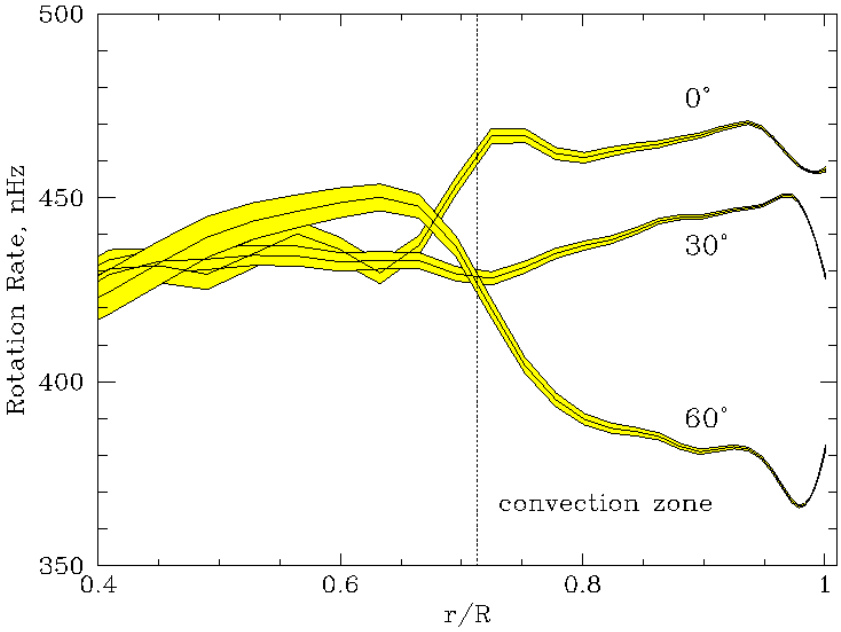


Figure 2.17: The diagram shows the solar rotation rate inferred from two months of SOHO/MDI data as a function of radius at three latitudes, 0 degrees, 30 degrees, and 60 degrees. 350 nHz corresponds to a 33-day rotation rate and 450 nHz to a 26-day rate. The data are spatial averages of the full-disk Doppler velocity out to ninety percent of the Sun's radius, measured each minute. This MDI observational program results in 23,000 bins of approximately ten arcsecond resolution, which, in turn, provides sensitivity to solar p mode frequency oscillations up to degree l=300 of the spherical surface harmonic modes. (From Internal Structure and Rotation of the Sun: First Results from the MDI Data, by A.G. Kosovichev et al., see http://soi.stanford.edu/results/srotation.html)

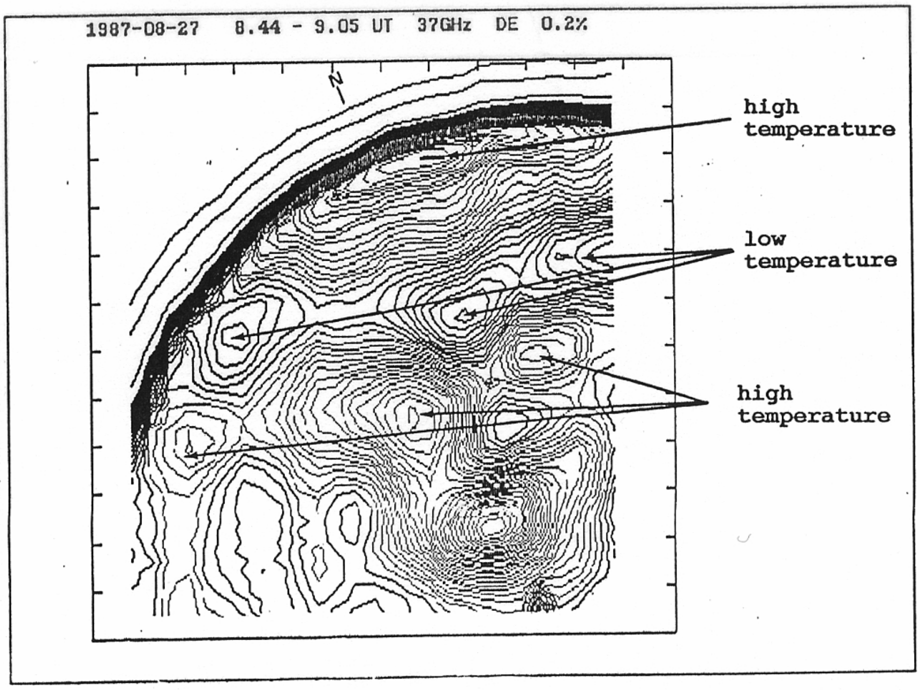


**FIGURE 2:** Enlarged solar map showing the north pole with low temperature areas below the enhanced polar region. Map measured at Metsahovi on August 27, 1987. Contours 0.2 % of the quiet Sun level.

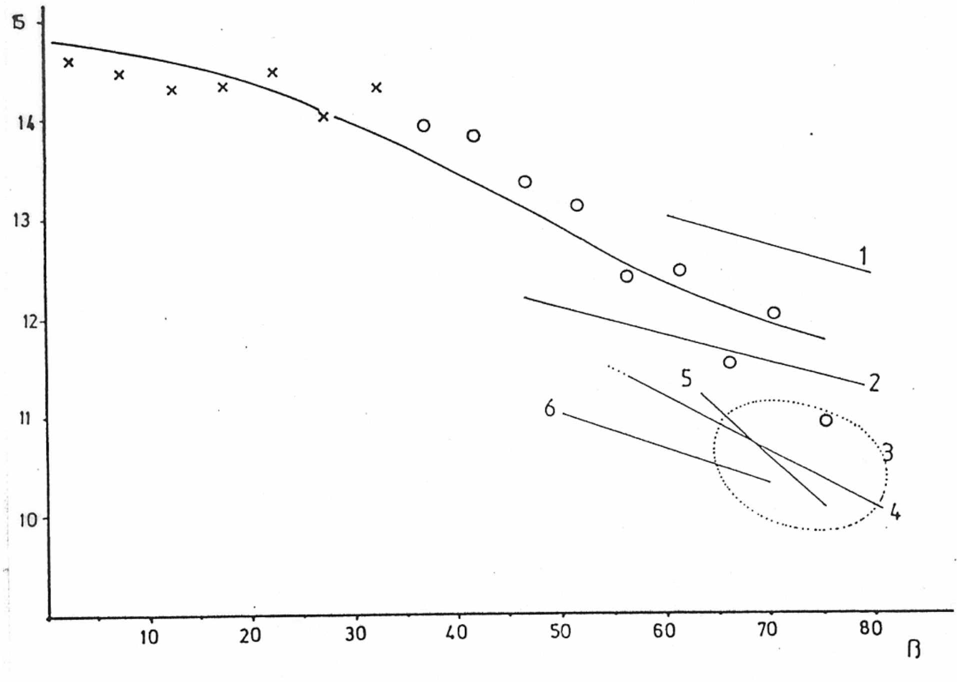


**FIGURE 3:** Curves of the sidereal rotation rate (deg/day) vs. solar latitude.

+) filaments, Adams & Tang (1977)
circles) polar crown filaments, Brajsa et al. (1990)
1) filaments, d'Azambuja (1948), after Schroter (1985)
2) & 3) polar faculae, after Makarova & Solonsky (1987)
4) photosphere, spectroscopic, Howard & Harvey (1970)
5) polar faculae, Waldmeier (1955) & Muller (1954), after Hansen et al. (1969)
6) high temperature regions at 37 GHz, present work

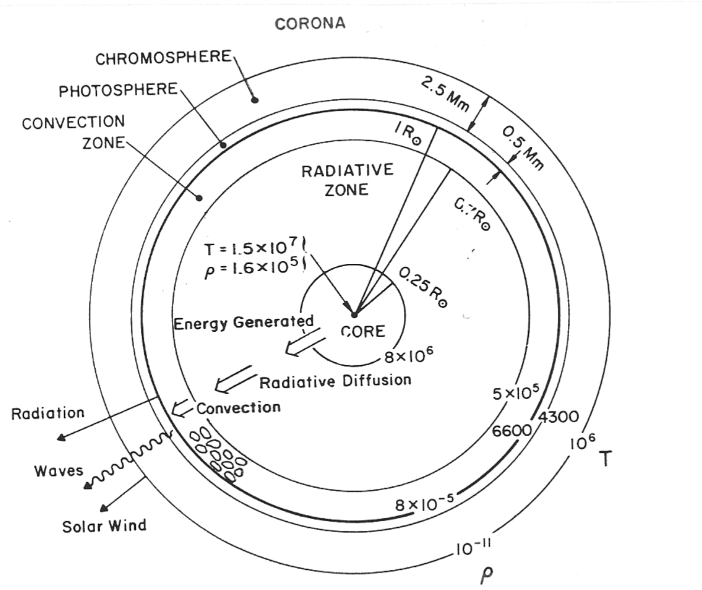


Figure 2.18: A schematic drawing of the solar structure.

## 2.9 Solar atmosphere

Solar atmosphere can be divided into three different layers (based on the temperature and density variation), and they are called photosphere, chromosphere, and corona. Photosphere is the 'light sphere', a thin layer (500 km) which is often taken as the sun's surface as it is what we see when we look at the sun in white (= visible) light. Within the photosphere, the temperature drops from 6400 K to about 4400 K, and then starts to rise again. When we measure magnetic fields using Zeeman splitting, the lines are photospherically-formed Fraunhofer lines, and the magnetic field strengths are only valid for the photosphere. Chromosphere, the 'colour sphere', is a 1500 km thick layer above the photosphere, where temperature first rises gradually and then sharply. (In fact the thin region between the chromosphere and corona is called the transition region, to emphasize the change.) The rich variety of chromospheric spectral lines provides a lot of observational material, especially in EUV. Corona, the 'crown', has a temperature of a few million degrees, and it emits strongly in radio and X-rays. Why the corona has such a high temperature is not known exactly, and this is called the coronal heating problem. Coronal gas has a low density and the gas is almost fully ionized. Electrons are 'frozen' into the solar magnetic field, but they can move away from the sun within the solar wind or during coronal mass ejections and other eruptions.

The structure of the solar magnetic field changes within the activity cycle. During minimum activity, a streamer belt is observed near the equator, but it changes into a more complex structure during activity maximum. Current sheets can be observed in association with helmet streamers. Since a neutral line separates magnetic fields of opposite polarity, a current must flow inside it, and thus a neutral line is a current sheet - and the sheet is observed to extend outward through the tips of the helmet streamers.

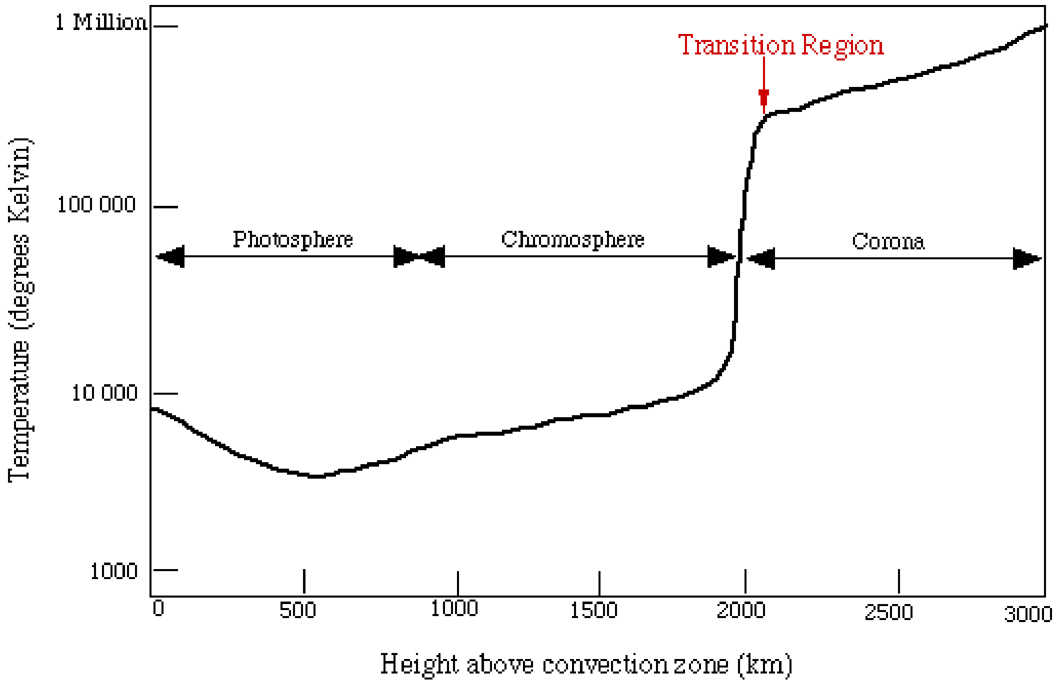


Figure 2.19: The solar atmosphere (adapted by M.B. Larson from Kenneth Lang: Sun, Earth, Sky).

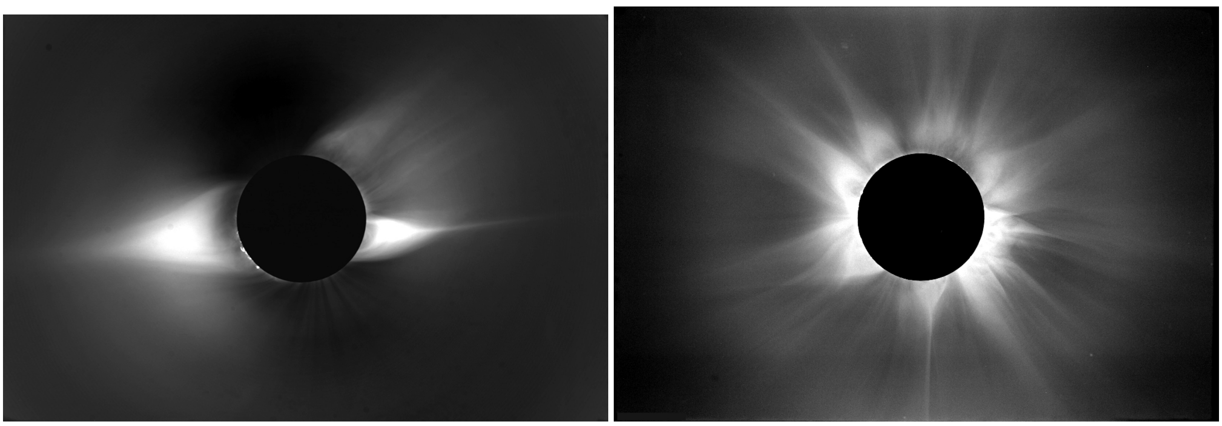

Figure 2.20: Coronal streamers are permanent features but their number also depends on the activity cycle. Left: eclipse photograph during activity minimum and Right: during activity maximum (High Altitude Observatory).

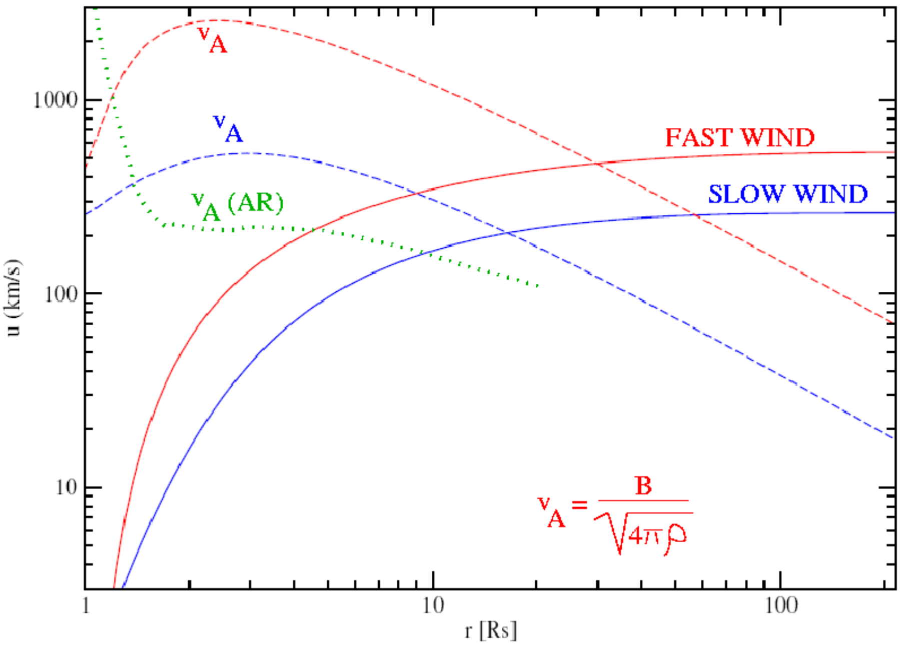


Figure 2.21: Alfvén speed ($v_A$) and solar wind speed in the (quiet sun) solar atmosphere and above an active region (AR). Speeds are in km/s. In X-axis is the distance $Rs$ from the solar surface (limb) in solar radiae (at the limb, $Rs = 1$). Alfvén speed depends on the magnetic field strength $B$ and electron density $\rho$. Within an active region and low in the atmosphere, magnetic field strengths are high and thus also Alfvén speeds are high. Outside the active regions (in 'quiet sun' atmosphere), density decrease is faster than the decrease in $B$, and hence the Alfvén speed rises in the low corona, up to a distance of $3-5\ Rs$. (Original plot from Timo Laitinen)

## 2.10 Plasma diagnostics

For a fully ionized plasma, in known conditions within the solar system, we can use the following approximations (all in gaussian units; density in $\mathrm{cm}^{-3}$ and field strength in G):

plasma frequency

$$\nu_p \approx 9 \times 10^3 \sqrt{n_e} \qquad \text{(Hz)}, \tag{2.6}$$

Alfvén speed (in hydrogen plasma, primordial abundances; transverse wave that propagates parallel to the magnetic field and does not compress the plasma)

$$v_A \approx \frac{2 \times 10^{11} B}{\sqrt{n_e}} \qquad \text{(cm/s)}, \tag{2.7}$$

sound speed (longitudinal wave that propagates parallel to the magnetic field and compresses the plasma)

$$v_s \approx 1.5 \times 10^4 \sqrt{T} \qquad \text{(cm/s)}, \tag{2.8}$$

magnetosonic speed (longitudinal wave that propagates perpendicular to the magnetic field, also known as the compressional Alfven wave or magnetoacoustic wave)

$$v_{ms} = \sqrt{v_s^2 + v_A^2}, \tag{2.9}$$

plasma $\beta$ is the ratio of the plasma pressure to the magnetic pressure

$$\beta = \frac{16\pi nkT}{B^2}. \tag{2.10}$$

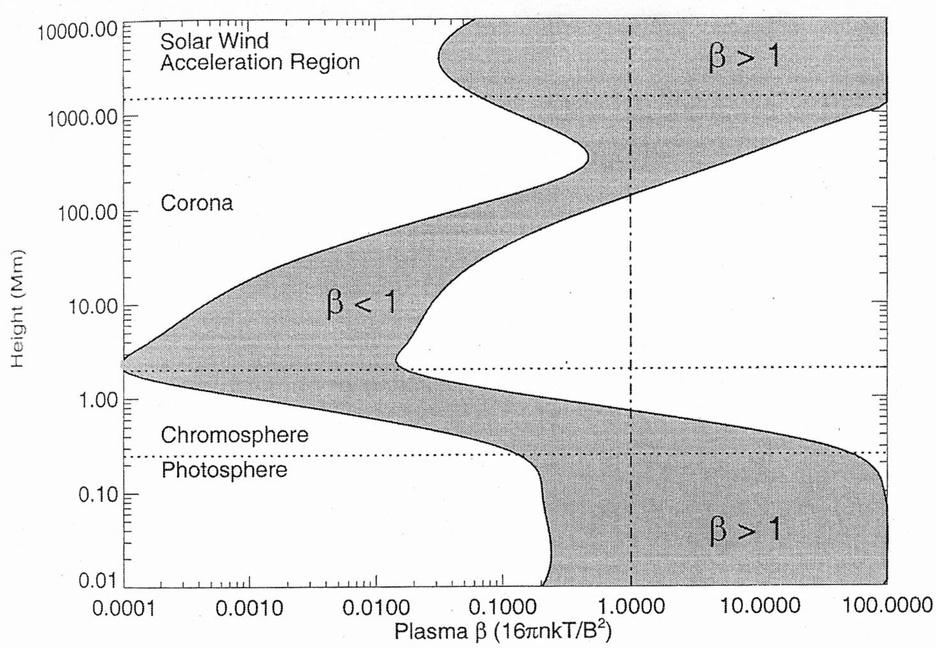


Figure 2 Plasma $\beta$ in the solar atmosphere for two assumed field strengths, 100 G and 2500 G. In the inner corona ($R \lesssim 0.2R_{\odot}$), magnetic pressure generally dominates static gas pressure. As with all plots of physical quantities against height, a broad spatial and temporal average is implied. (Courtesy of G. Allen Gary.)

Figure 2.22: Plasma $\beta$ in the solar atmosphere. Coronal loops contain hot and dense plasma (high value of $\beta$) while the corona itself is less dense but extremely hot and only weakly magnetized (low $\beta$ value). This may give rise to instabilities (so-called ballooning instability). The 'high-$\beta$ disruption' has been proposed to be the reason why plumes disintegrate.

## 2.11 Atmospheric densities

Atmospheric density models are used to describe density changes at different heights. As plasma frequency depends on the local density, these values are of interest especially to solar radio astronomers.

The Newkirk (1961) density model is based on hydrostatic equilibrium and the density values stay high also at large distances from the sun

$$n = 4.2 \times 10^4 \times 10^{4.32/r}, \tag{2.11}$$

here the distance $r$ is expressed in solar radius $R_\odot$, measured from the center of the sun, and electron density is in $cm^{-3}$.

The Saito (1970) model describes best quiet sun densities near the equator,

$$n = k1 \times r^{-16} + k2 \times r^{-6} + k3 \times r^{-2.5} \quad (2.12)$$

where $k1 = 3.09 \times 10^8$, $k2 = 1.58 \times 10^8$, and $k3 = 0.0251 \times 10^8$, units as in the Newkirk model.

Because both of these 'basic' density models fail to work in active region densities, they are usually multiplied with selected constants: for example a 2-times Newkirk model means $n = 2 \times 4.2 \times 10^4 \times 10^{4.32/r}$. A 10×Saito can be used within active regions, but it does not work at large distances from the sun. Measurements of coronal densities would be most useful, but they are infrequent and the analysis of coronal images is difficult (coronal images show scattered white light).

The interplanetary (IP) approximation is based on the relation $n_e \sim R^{-2}$, and gives

$$n_e = \frac{n_0}{R_d^2} \quad (2.13)$$

where $n_0$ ($cm^{-3}$) is the plasma density near Earth (at 1 AU) and $R_d$ (AU) is the distance from the sun. This model does not work well in the solar corona, since the densities it gives are too low. There are also 'hybrid' models that try to combine the different characteristics, e.g. by Vrsnak et al. (2004) which starts as a 5-times Saito at solar surface and continues as the modified IP model by Leblanc et al. (1998) towards the Earth.

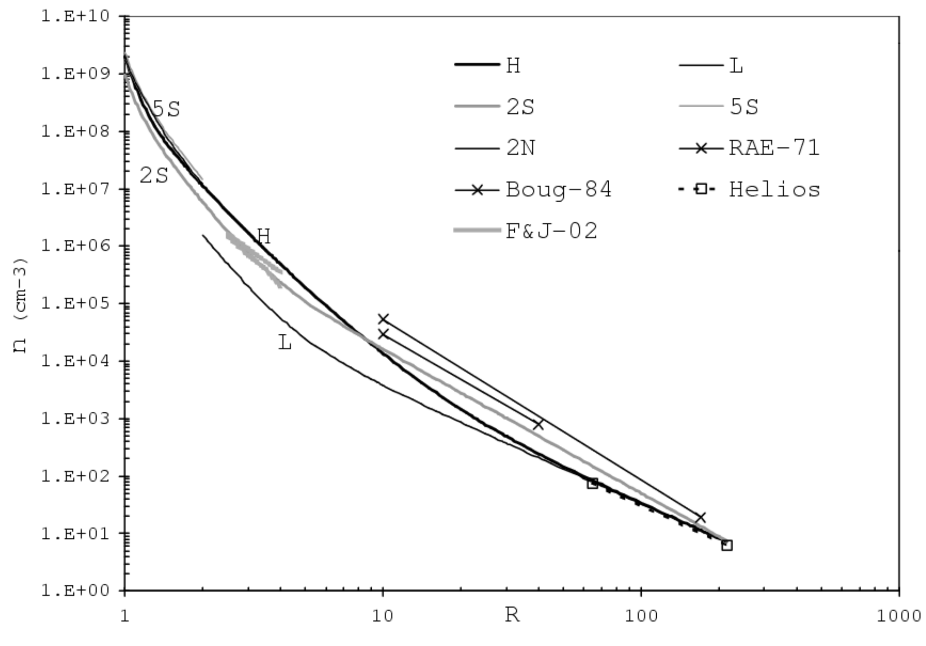


Figure 2.23: Density models from the AR-corona to IP space: H - the hybrid density model by Vrsnak et al. (A&A 413, 753, 2004); L - the model by Leblanc et al. (1998); 2S and 5S - two-fold and five-fold Saito (1970) model; RAE-71 - Fainberg & Stone (1971); Boug-84 - the results by Bougeret et al. (1984b) as given in Bougeret et al. (1984a); Helios - in situ measurements (Bougeret et al. 1984a); F&J-02 - Frazin & Janzen (2002).

Table 2.1: Calculated electron densities and plasma frequencies (wavelengths in parenthesis) at different distances $h$ ($R_\odot$) from the center of the sun ($R_\odot$=1 at the limb).

| $f_p$ (MHz) | $\lambda$ (m) | $n_e$ ($cm^{-3}$) | h Saito | h Hybrid | h 2×Newkirk | h 10×Saito | h Leblanc[a] | h IP[a] |
|---|---|---|---|---|---|---|---|---|
| 500 | 0.6 | $3.1\times10^9$ | - | - | - | 1.035 | - | - |
| 400 | 0.75 | $2.0\times10^9$ | - | - | - | 1.076 | - | - |
| 300 | 1 | $1.1\times10^9$ | - | 1.044 | 1.050 | 1.142 | - | - |
| 200 | 1.5 | $4.9\times10^8$ | - | 1.117 | 1.147 | 1.258 | - | - |
| 100 | 3 | $1.2\times10^8$ | 1.131 | 1.305 | 1.368 | 1.560 | - | - |
| 70 | 4.3 | $6.0\times10^7$ | 1.226 | 1.453 | 1.514 | 1.758 | - | - |
| 50 | 6 | $3.1\times10^7$ | 1.342 | 1.637 | 1.682 | 1.989 | 1.10 | - |
| 30 | 10 | $1.1\times10^7$ | 1.584 | 2.010 | 2.040 | 2.403 | 1.31 | - |
| 14 | 21.4 | $2.4\times10^6$ | 2.07 | 2.78 | 2.96 | 3.33 | 1.71 | - |
| 12 | 25 | $1.8\times10^6$ | 2.19 | 2.96 | 3.24 | 3.57 | 1.80 | - |
| 10 | 30 | $1.2\times10^6$ | 2.36 | 3.24 | 3.74 | 3.97 | 1.93 | - |
| 9 | 33.3 | $1.0\times10^6$ | 2.44 | 3.38 | 4.00 | 4.17 | 2.00 | - |
| 8 | 37.5 | $7.9\times10^5$ | 2.56 | 3.57 | 4.44 | 4.47 | 2.09 | - |
| 7 | 42.9 | $6.0\times10^5$ | 2.72 | 3.81 | 5.05 | 4.86 | 2.20 | - |
| 6 | 50 | $4.4\times10^5$ | 2.90 | 4.10 | 6.00 | 5.38 | 2.33 | - |
| 5 | 60 | $3.1\times10^5$ | 3.13 | 4.46 | 7.61 | 6.06 | 2.49 | - |
| 4 | 75 | $2.0\times10^5$ | 3.49 | 4.96 | 11.46 | 7.09 | 2.72 | 1.02 |
| 3 | 100 | $1.1\times10^5$ | 4.07 | 5.75 | >30 | 8.88 | 3.07 | 1.37 |
| 2 | 150 | $4.9\times10^4$ | 5.18 | 7.07 | >> | 12.17 | 3.69 | 2.06 |
| 1 | 300 | $1.2\times10^4$ | 8.58 | 10.36 | >> | 21.30 | 5.42 | 4.16 |

**a)** $n_0$=4.5 $cm^{-3}$ at 1 AU

## 2.12 Magnetic field strengths

We can approximate the magnetic field strengths in the solar corona as in Vainio & Khan (ApJ, 2004), the approximation is valid for equatorial regions:

$$B \sim 1.7\left(\frac{R_\odot}{R}\right)^3 + 1.3\left(\frac{R_\odot}{R}\right)^2 (G). \tag{2.14}$$

The empirical scaling law presented by Dulk & McLean (Solar Physics, 1978) gives the strength of the coronal magnetic field above active regions and it works best at distances 1.02 – 10 $R_\odot$:

$$B = 0.5 \times h^{-1.5}(G), \tag{2.15}$$

where $h$ is the height above the photosphere expressed in solar radiae. Field strengths of 22 G would then appear at about heights of 56 000 km and 10 G at about 95 000 km.

Using radio observations of gyrosynchrotron emission, the field strengths can be calculated if other source parameters (volume, density and viewing angle) are known. However, in most cases we can just give most probable range values for the fields.

Magnetic field strengths at sunspot centers can be approximately 1000 – 3000 Gauss. In the solar corona the field strengths are 10 – 300 G (similar to fridge magnets, at 200 G). At Earth, the magnetic field strength is about 0.5 G.

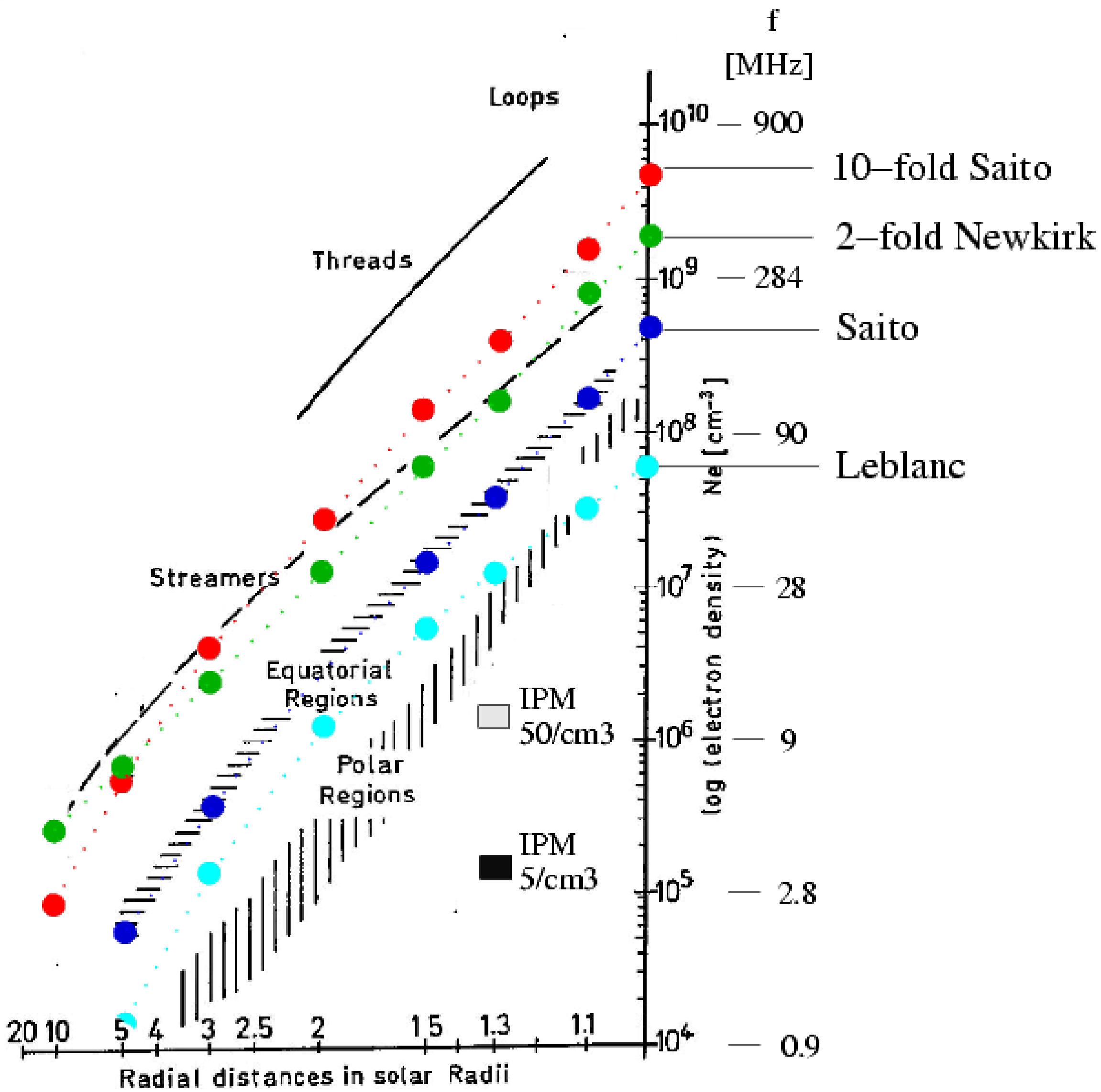


Figure 2.24: Electron densities in the solar corona: dashed areas are based on eclipse observations (S. Koutchmy) and the filled circles describe the densities given by different models (Saito, Newkirk, Leblanc et al.). The two filled boxes show densities given by the IP density models, with two different densities near Earth: 5 $cm^{-3}$ during activity minimum and 50 $cm^{-3}$ during activity maximum.